Roles of oceanic ventilation and terrestrial outflow in the atmospheric non-methane hydrocarbons over the Chinese marginal seas

Jian Wang[1], Lei Xue[2], Qianyao Ma[1], Feng Xu[1], Gaobin Xu[1], Shibo Yan[1], Jiawei Zhang[3], Jianlong Li[1], Honghai Zhang[1, *], Guiling Zhang[1], Zhaohui Chen[4]

[1]Frontiers Science Center for Deep Ocean Multispheres and Earth System, Key Laboratory of Marine Chemistry Theory and Technology, Ministry of Education, and College of Chemistry and Chemical Engineering, Ocean University of China, Qingdao 266100, China

[2]Department of Chemistry, College of Environmental Science and Forestry, State University of New York, Syracuse, NY, 13210, United States

[3] Eco-Environmental Monitoring and Research Center, Pearl River Valley and South China Sea Ecology and Environment Administration, Ministry of Ecology and Environment, Guangzhou 510610, China

[4]Key Laboratory of Physical Oceanography, Ministry of Education, Ocean University of China, Qingdao 266100, China

* To whom correspondence should be addressed: honghaizhang@ouc.edu.cn

Abstract

Non-methane hydrocarbons (NMHCs) in the marine atmosphere have been extensively studied due to their important roles in regulating the atmospheric chemistry and climate. However, very little is known about the distribution and sources of NMHCs in the lower atmosphere over the marginal seas of China. Herein, we characterized the atmospheric NMHCs (C2-C5) in both the coastal cities and marginal seas of China in spring 2021, with a focus on identifying the sources of NMHCs in the coastal atmosphere. The NMHCs in urban atmospheres, especially for alkanes, were significantly higher compared to that in the marine atmosphere, suggesting that terrestrial NMHCs may serve as an important reservoir/source of the marine atmosphere. A significant correlation was observed between the alkane concentrations and the distances from sampling sites to the nearest land or retention of air mass over land, indicating that alkanes in the marine atmosphere are largely influenced by terrestrial inputs through air-mass transport. For alkenes, a greater impact from oceanic emissions was determined due to the lower terrestrial concentrations, short atmospheric lifetime, and substantial sea-to-air fluxes of alkenes compared to alkanes (489 ± 454 vs 129 ± 106 nmol m^{-2} d^{-1}). As suggested by the positive matrix factorization, terrestrial inputs contributed to 89 % of alkanes and 69.6 % of alkenes in Chinese marginal seas, subsequently contributing to 84 % of the ozone formation potential associated with C2-C5 NMHCs. These findings underscore the significance of terrestrial outflow in controlling the distribution and composition of atmospheric NMHCs in the marginal seas of China.

Keywords: non-methane hydrocarbons, oceanic ventilation, terrestrial outflow, source apportionment

1 Introduction

Non-methane hydrocarbons (NMHCs), a significant subset of volatile organic compounds (VOCs), are acknowledged as key precursors to tropospheric ozone formation (Houweling et al., 1998; Solomon et al., 2005) and organic aerosol generation (Hallquist et al., 2009; Wu and Xie, 2018), playing a pivotal role in atmospheric chemistry. The presence and activity of NMHCs in the troposphere have far-reaching implications, not only influencing the dynamics of ozone and organic aerosol formation but also significantly impacting air quality. These compounds are intricately linked to heightened human health risks as well as possessing indirect yet profound effects on the broader climate system through their interactions with various atmospheric processes (Yuan et al., 2018).

The emission of NMHCs into the atmosphere stems from an array of natural and anthropogenic processes. Oceanic sources of NMHCs predominantly entail the biogenic production of phytoplankton and photochemical degradation of dissolved organic matter (DOM) (Bonsang et al., 1992; Li et al., 2019; Riemer et al., 2000; Sahu et al., 2010). However, they are minimal when compared to terrestrial inputs. Despite the uncertainties in the global flux of VOCs, substantial evidence indicates a significant discrepancy between terrestrial emissions (660-1146 Tg C yr^{-1}) (Guenther et al., 1995, 2012; Messina et al., 2016; Sindelarova et al., 2014; Singh and Zimmerman, 1992) and marine emissions (5-36 Tg C yr^{-1}) (Guenther et al., 1995; Singh and Zimmerman, 1992). A substantial amount of NMHCs originating from terrestrial sources (e.g., vehicular emissions, biomass combustion, industrial activities, and continental vegetation emissions) can be transported into the offshore atmosphere via air mass conveyance (Wang et al., 2005; Kato et al., 2007; Song et al., 2020). Subsequently, these

3

66   supplementary terrestrial NMHCs will play a pivotal role in shaping the chemical

67   composition of the offshore atmosphere and influencing local environmental dynamics.

68   Hence, to further understand the characteristics, variation, and origins of NMHCs in the

69   offshore atmosphere, it is imperative to scrutinize oceanic emissions and meanwhile, it

70   is necessary to figure out the effect of terrestrial outflow on nearshore NMHCs.

71   The Yellow Sea and the East China Sea are important parts of Chinese marginal seas,

72   situated along the eastern coast of China where it is densely populated and has intensive

73   industries. The rapid pace of Chinese development has seen a notable escalation in

74   anthropogenic NMHCs emissions over recent decades (He et al., 2019). Presently,

75   excessive NMHCs emissions and severe ozone pollution have emerged as urgent

76   environmental challenges in China, particularly in highly urbanized and industrialized

77   areas along the eastern coast (Liu et al., 2016; Zhang et al., 2018). The seasonal cycle

78   of the Asian monsoon and diurnal fluctuations of sea-land breezes can facilitate the

79   transport of terrestrial pollution to the marine atmosphere (Ding et al., 2004; Wang et

80   al., 2003; Talbot et al., 2003; Russo et al., 2003). Additionally, eutrophication in coastal

81   regions fosters the proliferation of phytoplankton, potentially augmenting the natural

82   emissions of NMHCs. Consequently, conducting atmospheric investigations in the

83   coastal region of eastern China is effective in revealing the potential effects of land-sea

84   interactions on offshore atmospheric NMHCs.

85   In the spring of 2021, atmospheric samples were systematically collected from both

86   coastal cities and marginal seas of China, providing representative insights into the

87   characteristics of NMHCs (C2-C5) and facilitating discussion on the interplay between

88   ocean emission and terrestrial outflow concerning atmospheric NMHCs. Ultimately,

89   the contributions of diverse sources to NMHCs were quantified using the positive

90   matrix factorization (PMF) model, with assistance from indications provided by other

typical gases, mainly dimethyl sulfur (DMS), volatile halogenated compounds (VHCs), and monocyclic aromatics.

2 Methods

2.1 Samples collection

The urban samples were collected from eight coastal cities in China from March 27 to April 1, 2021 (Fig. 1). Air samples were collected using fused silica-lined canisters (2.5 L), which were cleaned three times via a Canister Cleaning System (2101DS, Nutech) and were pumped into a negative pressure state before sampling. The sampling sites were selected at the top of high buildings to minimize contamination of particular point sources. Air samples were collected at 09:00 and 21:00 local time (UTC+8) aimed to represent the urban atmospheric conditions during the daytime and night, respectively. Note that night samples in Xiamen and Qinzhou were missing.

Oceanic air samples were collected aboard RV "*Dong Fang Hong 3*" during the voyage in the Yellow Sea and the East China Sea from April 17 to May 2, 2021. Nineteen oceanic air samples were collected on the top deck facing the wind when the ship was about to arrive at the station and started to slow down. Seawater samples were collected via prewashed Niskin bottles (12 L) incorporated into the Conductivity-Temperature-Depth Sensor Rosette (Seabird 911). Sampling details for urban (Table S4) and marine samples (Table S5) are shown in supplementary tables.

2.2 Analysis of air samples

For the measurement of most types of gases, air samples were processed immediately after being brought back to the laboratory, using an Atmospheric Pre-concentrator

System (8900DS, Nutech) coupled with a GC-MSD system (GC-7890A, MSD-5975, Agilent). The pretreatments of air samples were as follows. First, the Atmospheric Pre-concentrator System was baked for 10 min to clean the interior instrument. Then trap 1 was cooled to -170 °C using liquid N_2 and a 300 mL air sample was pumped from the canister into trap 1 for the initial concentration of the target compounds, while N_2 and O_2 escaped due to their lower boiling points. After trap 2 was cooled to -50 °C, trap 1 was heated to 30 °C to transfer the target compounds from trap 1 to trap 2. Moisture and CO_2 were removed in the second concentration. Then, trap 2 was warmed up to transfer the target compounds into the last trap for cryofocusing (-175 °C). Finally, the last trap was instantaneously heated to 200 °C via gas bath heating, and the target compounds were delivered into the GC-MSD system by ultra-pure He.

For the parameter settings of GC-MSD, the temperature of the inlet, quadrupole, and ionization source was 150 °C, 150 °C, and 230 °C, respectively. The inlet was set to split mode with a ratio of 10:1. The flow rate of carrier gas (He) was set to 1.5 mL min^{-1} in the instant flow mode. Specific columns were selected to separate the NMHCs (Rt-Alumina BOND/KCl, Restek), monocyclic aromatics (DB-624, Agilent), DMS (CP7529, Agilent), and VHCs (DB-624, Agilent). Gas standards of NMHCs in N_2 (Linde Gases, Germany) were diluted to 0.1-1 ppb for identification and calibration. Details of temperature programming and detector parameters can be seen in Zou et al. (2021) and Li et al. (2019). The precision and detection limits for the trace gases in the present study were 1-7 % and 0.03-20.0 ppt, respectively (Table S1). Specifically, carbon monoxide (CO) was analyzed on-site using a trace gas analyzer (TA3000R, Ametek) with a lower detection limit of 10 ppb; more details can be found in Xu et al. (2023). Note that data on DMS, CO and VHCs from marine atmospheric samples were graciously provided by colleagues in the same laboratory. These data were used only as

supporting information in the interpretation of our core dataset in this paper (e.g., correlation analysis).

2.3 Analysis of seawater samples

C2-C5 NMHCs in seawater were measured immediately on board using a purge and trap system coupled with the gas chromatography equipped with a flame ionization detector (GC-FID, 7890B, Agilent). The purge and trap system was improved based on a previously self-designed device described by Li et al. (2019). Briefly, seawater was collected using a customized glass sampler (500 mL) and was connected to the inlet of the system. Then seawater was transformed into the extraction cell under the pressure of pure N_2 and was purged with pure N_2 bubble flow (250 mL min^{-1}). The moisture of the carrier gas condensed in a thin glass tube that was placed in a cold chamber (4-6 °C) and the carbon dioxide was absorbed by the glass tube filled with Ascarite II (Merck). The targets were concentrated in a passivated stainless-steel tube immersed in liquid nitrogen for 26 mins. Then, the steel tube was heated by boiling water and immediately, the six-way valve was turned for the inlet situation. The concentrated target compounds were transferred into the Rt-Alumina BOND/KCl capillary column for separation and were determined by the FID. The parameters of the inlet, oven, and detector are shown in Table S2. The gas standard (Linde Gases, Germany) was diluted with ultra-pure N_2 to 10 ppb for identification and quantification. The instrumental blank was made to guarantee data reliability. The precision and detection limits were 3-6 % and 0.5-1.0 pmol L^{-1} (Table S3).

2.4 Calculation of sea-to-air flux

The sea-to-air flux of each NMHCs (F, nmol m^{-2} d^{-1}) was calculated using Eq. (1):

$$F = k \times (C_w - C_a \times H) \tag{1}$$

where k (m s^{-1}) is the gas transfer velocity described by Eq. (2); H is Henry's law

constant; C_w (pmol L^{-1}) and C_a (ppb) are concentrations of each NMHCs in the

surface seawater (5 m depth) and atmosphere, respectively.

$$k = 0.31 \times u^2 \times (\frac{Sc}{660})^{-0.5} \tag{2}$$

where u (m s^{-1}) is the wind velocity at 10 m. Sc is the Schmidt number and is defined

as Sc = v/D. v was the kinematic viscosity of seawater calculated by Eq. (3)

(Wanninkhof, 1992). D is the gas diffusion coefficient related to temperature described

by Eq. (4) (Wilke and Chang, 1955).

$$v = 1.052 + 1.300 \times 10^{-3} \times t + 5.000 \times 10^{-6} \times t^2 + 5.000 \times 10^{-7} \times t^3 \tag{3}$$

$$D = \frac{7.4 \times 10^{-8} (q \times M_b)^{0.5} \times T}{n_b \times V_a^{0.6}} \tag{4}$$

where t (°C) is the degree Celsius of seawater, q is the association factor of water,

M_b (g mol^{-1}) is the molar weight of water, T (K) is the degree Kelvin of seawater, n_b

is the dynamic viscosity of seawater and V_a is the molar volume at the boiling point.

2.5 Calculation of OFP and P$_{SOAP}$ of NMHCs

To assess the environmental implications of NMHCs, the ozone formation potential

(OFP, µg m^{-3}) and secondary organic aerosol (SOA) formation potential (P_{SOAP}, µg m^{-3}) are calculated using Eq. (5) and Eq. (6), respectively (Carter, 1994).

$$OFP_i = MIR_i \times C_i \tag{5}$$

$$P_{SOAPi} = \sum C_i \times SOAP_i \times FAC_{toluene}/100 \tag{6}$$

Where C_i represents the concentration of NMHCs; MIR_i (g O₃/g VOCs) and $SOAP_i$

(relative to toluene = 100) are constants that represent the maximum incremental

reactivity and SOA potential of i, respectively (Carter, 2010); $FAC_{toluene}$ is the

fractional aerosol coefficient of toluene, which has a value of 5.4% (Grosjean and

185 Seinfeld, 1989). Specific data was listed in supplementary Table S11.

186 **2.6 Normalized concentrations and lifetime-weighted concentrations of NMHCs.**

187   To effectively compare the NMHCs variation with respect to the distance from the

188 sampling sites to the land (like Fig. 2d, f), we calculated the normalized concentration

189 for each NMHCs (C_{Nor-i}) using Eq. (7).

190 $$C_{Nor-i} = \frac{c_i}{c_{max-i}} \tag{7}$$

191 where C_i is the concentration of gas i and C_{max-i} is the maximum of gas i.

192   A novel approach was employed to analyze the correlation between the

193 concentrations of various NMHCs and their sea-to-air fluxes. Concentrations were

194 weighted according to the respective atmospheric •OH lifetime of each NMHCs. This

195 was achieved by dividing the concentration of each NMHCs by its corresponding

196 atmospheric •OH lifetime, yielding a "lifetime-weighted concentration" for each

197 NMHCs (C_{life-i}) (Eq. 8). This method provides a more nuanced understanding of the

198 impact of oceanic emission on NMHCs, taking into account not only their abundance

199 but also their residence in the atmosphere.

200 $$C_{life-i} = \frac{c_i}{\tau_i} \tag{8}$$

201 where C_i is the atmospheric concentration of gas i, τ_i is the •OH lifetime of gas i.

202 The approximate atmospheric lifetime of each NMHCs was calculated assuming an

203 average [•OH] of 6×10^5 molecules cm^{-3} within 24 h at 288 K (Jobson et al., 1999), with

204 specific data listed in Table 1.

205 **2.7 Calculation of the shortest distance from the sampling station to the land**

206   Coastline latitude and longitude data near the study area (20-45°N, 110-130°E) were

207 extracted from the World Vector Shorelines (downloaded from

2.8 Calculation of retention of air mass over land

To identify whether an air mass was mainly from terrestrial or oceanic regions, the retention ratio of the air mass over land (R_L) was calculated by Eq. (9).

$$R_L = \frac{\sum_{n=1}^{N_{land}} e^{-\frac{t_n}{48}}}{\sum_{n=1}^{N_{total}} e^{-\frac{t_n}{48}}} \tag{9}$$

Where N_{total} is the total number of trajectory endpoints (downloaded from NOAA Air Resources Laboratory HYSPLIT trajectory model https://www.arl.noaa.gov/). N_{land} is the total number of trajectory endpoints located over land, while t_n is the backward tracking time with the unit of hour and $e^{-\frac{t_n}{48}}$ is the weighting factor related to tracking time as the diffusion of air mass takes place along the transport path than in the nearby regions. As a result, the larger R_L value indicates that the air mass is more influenced by terrestrial transport and its source is more likely to be on land. Similar methods have been used to calculate the average residence time of sampled air masses in the Arctic (Willis et al., 2017) and identify the percentage of time spent by trajectories over different surface types in the Antarctic (Decesari et al., 2020). R_L values were calculated by three different time-scale trajectories (48h, 72h, and 96h) (listed in Table S9). The mean R_L (n = 3) was finally applied to analyze the terrestrial influence on oceanic NMHCs, mitigating the uncertainty caused by the trajectory with different time-scales.

2.9 Application of the PMF model

PMF model introduced in detail in the study of Paatero and Trapper (1994) was applied to analyze the data of atmospheric NMHCs in the Yellow Sea and the East China Sea. Based on a matrix consisting of the concentrations of diverse chemical species, the objective of PMF is to determine the number of NMHCs source factors, the chemical composition profile of each factor, and the contribution of each factor to species. The matrix representation of this model is as Eq. (10).

$$x_{ij} = \sum_{k=1}^{p} g_{ik} f_{kj} + e_{ij} \tag{10}$$

Where x_{ij} represents the concentration of species j measured on sample i, p denotes the number of factors facilitating the samples. f_{kj} represents the concentration of species j in factor profile k, g_{ik} denotes the relative contribution of factor k to sample i, and e_{ij} represents the PMF model error of species j measured on sample i. The factors resolved by PMF are typically interpreted as sources. The objective of this algorithm is to find the values of f_{kj}, g_{ik}, and p that best reproduce x_{ij}, continuously adjusting f_{kj} and g_{ik} until the minimum Q value for a given p is attained. Q is defined as Eq. (11).

$$Q = \sum_{i=1}^{n} \sum_{j=1}^{m} \left(\frac{e_{ij}}{\sigma_{ij}} \right)^2 \tag{11}$$

Where σ_{ij} represents the uncertainty of the concentration of the species j in sample i, n is the number of samples, and m is the number of species. In applying the PMF model, the significance of missing data in the matrix was decreased by using the species median. The uncertainty for normal data was estimated as 20 % of the NMHCs concentrations because the analytical uncertainty was not available (Buzcu and Fraser, 2006). The model ran 20 times and we selected the result with the minimum Q value. Additionally, scaled residuals are instrumental in assessing the fit of the PMF model to

the observed data. They represent the difference between the observed and modeled data, scaled by the uncertainty in the observed data. In this PMF analysis, approximately 94 % of the scaled residuals ranged from -3 to 3 (Fig. S1), suggesting a reasonable fit of the model result.

3 Results and discussion

3.1 Atmospheric concentrations of NMHCs in coastal cities and marginal seas of China

To clarify, NMHCs determined in this study were separated into two groups for further discussion based on their distinctly different atmospheric reactivity and lifetimes: alkanes (long lifetime, 8.2-78 d) and alkenes (short lifetime, 0.19-2.3 d). In the urban atmosphere (n = 14), the mean (range) concentration of ethane, propane, i-butane, and n-butane was 2.26 ± 1.66 (0.277-5.72), 2.95 ±5.12 (0.149-20.1), 2.57 ± 6.99 (BD-27.6), and 3.29 ± 7.68 (0.018-30.2) ppb, respectively (Table 1). Alkanes combined accounted for ~76 %-99 % of total NMHCs measured in this study, which agrees with previous studies reporting alkanes as the dominant NMHCs in the urban atmosphere of China e.g., 43.7 % (Song et al., 2007), and > 50 % (Li et al., 2015). For alkene species in the urban atmosphere (n = 14), the mean (range) of ethylene, propylene, and isoprene was 0.180 ± 0.126 (0.035-0.390), 0.036 ± 0.040 (BD-0.129), and 0.046 ± 0.072 (0.006-0.250) ppb, respectively.

Similarly, alkanes were also dominant components in the marine atmosphere, accounting for ~86 %-95 % of NMHCs. In the marine atmosphere (n = 19), the mean (range) concentration of ethane, propane, i-butane, n-butane, ethylene, propylene, and isoprene was 1.24 ± 0.298 (0.686-1.72), 0.822 ± 0.518 (0.226-1.79), 0.283 ± 0.302 (BD-

1.17), 0.256 ± 0.214 (0.025-0.694), 0.151 ± 0.077 (0.028-0.295), 0.033 ± 0.009 (0.022-0.060), and 0.008 ± 0.010 (BD-0.043) ppb, respectively. These values were comparable to those reported in the Bengal Bay (Sahu et al., 2011) and the Northwest Pacific Ocean (Li et al., 2019) (Table S6). Alkanes in the urban atmosphere were on average more than four times higher than those in the marine atmosphere, while no significant difference was observed for concentrations of alkenes between urban and marine air (t = 2.224, p = 0.156) (Fig. 2a, b). In spatial terms, multiple NMHCs (e.g. ethane, propane, i-butane, n-butane, and ethylene) showed higher atmospheric concentrations in regions closer to the land. The elevated concentrations were primarily concentrated along the coastal regions of the East China Sea and the north Yellow Sea (Figure S3). The disparity in NMHCs concentrations between land and ocean, as well as the distribution pattern of NMHCs in the marine atmosphere, suggested the potential influence of terrestrial sources on the oceanic NMHCs.

3.2 Atmospheric NMHCs variability vs. estimated lifetime

The standard deviation of the natural logarithm of the NMHCs mixing ratios (S_{lnx}) was established to correlate to their •OH lifetime (τ) in the atmosphere following an exponential function of $S_{\text{lnx}} = A\tau^{-b}$ (Jobson et al., 1998), where A and b are fitting parameters. A b value approaching zero suggests that the NMHCs variability is primarily controlled by local emission fluctuations while a b value of 1 indicates the minimal impact of local emissions, with the variability predominantly controlled by the extent of photochemical reactions.

Employing the analytical framework in Jobson et al. (1998), we analyzed our atmospheric NMHCs data from urban areas and the Chinese marginal seas. The derived b value for urban areas was 0.05 (Fig. 3a), suggesting that atmospheric NMHCs in

301 coastal cities were mainly controlled by local emissions. In the marine atmosphere, the

302 b value was 0.26 (Fig. 3b) which was comparable to values reported for Gosan (0.30)

303 (Wong et al., 2007) and continental outflow from southern China (0.31) (Wang et al.,

304 2005), but it was significantly lower than the values for Ogasawara (0.43) (Kato et al.,

305 2004), the Northwest Indian Ocean (0.40) (Warneke and De Gouw, 2001), and the South

306 China Sea (0.42) (Wang et al., 2005). The b value of 0.26 in the atmosphere over the

307 Chinese marginal suggests that the NMHCs composition in the nearshore atmosphere

308 is influenced both by local oceanic emissions and the remote sources from the continent.

309 As sites closer to the source position tend to have lower b values, the Yellow Sea and

310 the East China Sea experience a more pronounced influence from terrestrial pollution

311 sources compared to Ogasawara, the South China Sea, and the Northwest Indian Ocean.

3.3 Terrestrial influence on marine atmospheric NMHCs variation

313 Given the discernible impact of terrestrial input on the spatial distributions and

314 variabilities of marine atmospheric NMHCs, we further elucidated the role of terrestrial

315 outflow in shaping marine atmospheric NMHCs levels. This examination focused on

316 three key factors: distance from the sampling site to the land, retention of air mass over

317 land, and transport time of air mass.

Distance from the sampling site to the land

319 The distances from the oceanic sampling sites to the nearest land spanned from 13.9

320 to 331 km, with an average of 123 km (Table S9). Significant correlations were

321 observed between the distances and concentrations of ethane (r = -0.553, n = 19, p =

322 0.014), propane (r = -0.605, n = 19, p = 0.006), i-butane (r = -0.513, n = 19, p = 0.025),

323 and n-butane (r = -0.573, n = 19, p = 0.010). When plotted against the distances, the

324   concentrations of alkanes combined decreased with the increasing distance (Fig. 2c),

325   and different species exhibited distinctly specific decreasing rates (Fig. 2d). Since the

326   concentrations between different NMHCs species varied considerably, the normalized

327   concentrations were employed to fit an attenuation equation ($y = Ae^{-tx}+y_0$) for each

328   species. As evident in Fig. 2d, the attenuation coefficients for ethane, propane, i-butane,

329   and n-butane were 0.003, 0.030, 0.031, and 0.022, respectively. These coefficients were

330   correlated with their atmospheric reactivities. Species with lower reactivity and longer

331   lifetimes, such as ethane (with a lifetime of 78 d), have the lowest attenuation

332   coefficient. This implies that long-lifetime species could be affected by the terrestrial

333   input even at a more remote marine site. Terrestrial influences on propane, i-butane,

334   and n-butane were discernible only in areas much closer to land, as their concentrations

335   stabilized at low values beyond a distance of around 100 km (Fig. 2d).

336   **Retention of air mass over land**

337   A larger retention of air mass over land (R_L) has previously been suggested to serve

338   as an indicator of a greater terrestrial influence (Zhou et al., 2021). To mitigate the

339   uncertainty derived from varying time-scale trajectories, we calculated the R_{L-mean}

340   based on 48, 72, and 96-hour backward trajectories. R_{L-mean} ranged from 0.10 to 0.96

341   (Table S9). When plotted against R_{L-mean}, a linear relationship was observed between

342   the concentrations of NMHCs combined and R_{L-mean}, with a slope of 2.51 (Fig. 4a).

343   A statistically significant correlation ($r = 0.599$, $n = 19$, $p = 0.007$) was observed when

344   only plotting alkanes with R_{L-mean}. However, the correlation between alkenes and

345   R_{L-mean} was statistically insignificant ($r = 0.248$, $n = 19$, $p = 0.306$).

Transport time of air mass

The transport time of air mass was estimated as the interval from the last point of the trajectory contacting the continent to the moment when the air mass reached the sampling location, as detailed by Kato et al. (2001). These times ranged from 4 to 81 h, with an average of 30 h (Table S9). A shorter air mass transport time signifies a stronger terrestrial influence, as NMHCs within the air mass undergo further oxidation and dispersion over time. Total NMHCs concentrations exhibited a significant decrease with the increase of air mass transport time, characterized by a slope of -0.04 (Fig. 4d). Alkanes displayed a steeper decline, indicated by a slope of -0.0079 (Fig. 4e) compared to alkenes (-0.0038, Fig. 4f). Notably, elevated alkane concentrations were affected by those air masses with larger R_{L-mean} (>0.8) and shorter transport time (<20 h) (Figure S4). This emphasized the terrestrial influence on alkanes in the marine atmosphere since both R_L and transport time serve as indicators of air mass terrestrial characteristics. However, similar to the analysis of R_L, the correlation between the air mass transport time and alkenes was statistically insignificant ($r = 0.248$, $n = 19$, $p = 0.306$).

Overall, the analysis above suggests that the terrestrial input plays an important role in driving the variability observed for the atmospheric NMHCs over the marginal seas of China. In particular, a stronger terrestrial impact was determined for the alkanes based on the larger slopes from linear regression analysis and the significant correlations with terrestrial indicators. In contrast, no discernible trend was found for alkenes when plotting their concentrations against the distance from sampling sites to the coastline (Fig. 2e, f). There was no significant correlation between alkenes and R_L or air mass transport time. Therefore, the variability of alkenes in the coastal atmosphere seems to be weakly impacted by the terrestrial sources when compared to alkanes. We attribute this to two main factors. First, the mean concentration of alkenes

in the urban air was only 1.4 times of that in marine air, whereas it was 5.4 times for alkanes. Alkenes undergo more rapid oxidation due to their higher reactivities compared to alkanes during air mass transport. Secondly, oceanic ventilation may play a more substantial role in affecting marine alkenes (discussed in section 3.4).

3.4 Oceanic impact on marine atmospheric NMHCs composition

Sea-to-air fluxes of NMHCs

The mean (range) of sea-to-air fluxes of ethane, propane, i-butane, n-butane, ethylene, propylene, and isoprene was 44.6 ± 35.0 (0.2-118), 41.5 ± 39.9 (0.2-157), 31.7 ± 38.2 (0.1-146), 10.9 ± 25.4 (-0.8-96.1), 321 ± 294 (1.7-775), 56.1 ± 55.2 (0.2-212), and 112 ± 134 (0.5-468) nmol m^{-2} d^{-1}, respectively, in the Yellow Sea and the East China Sea (Table 1). These values were comparable to those reported in Chinese marginal seas (Wu et al., 2021; Li et al., 2021) and 23-38°N Atlantic Ocean (Tran et al., 2013), but were larger than those reported values in the North Sea (Broadgate et al., 1997) and the Northwest Pacific Ocean (Li et al., 2019; Wu et al., 2023) (Table S10).

The averaged sea-to-air fluxes of alkanes and alkenes within 100 km from the coastline were 147 ± 116 and 551 ± 497 nmol m^{-2} d^{-1}, respectively, which were relatively higher than those beyond 100 km (Fig. 5a, b). Since there were no significant differences in surface seawater temperature and 10 m wind speed between regions within and beyond 100 km from the coastline (Fig. S5), the discrepancy in fluxes might not be driven by physical processes. These elevated fluxes in the sea areas closer to land could be attributed to the influence of phytoplankton biomass and chromophoric dissolved organic matter (CDOM). Seawater NMHCs are not only directly synthesized by phytoplankton (Ratte et al., 1995), but they can also be emitted through the photochemical degradation of CDOM (Ratte et al., 1993; Lee and Baker, 1992). To

substantiate our findings, we analyzed the monthly Chl-*a* concentration and the absorption coefficient at 443 nm of seawater in April 2021 from the remote sensing dataset from the NASA Ocean Color data service (https://oceancolor.gsfc.nasa.gov/) (Fig. S2). The mean (±SD) of Chl-*a* concentrations was 2.83 ± 1.17 and 1.68 ± 1.44 μg L^{-1} in the areas within and beyond 100 km from the coastline, respectively. Correspondingly, the mean (±SD) of seawater absorption coefficients at 443 nm was at 0.124 ± 0.060 and 0.069 ± 0.040 m^{-1}, respectively. Hence, the heightened phytoplankton biomass and enriched photoreaction substrate collectively enhanced both the biological production and abiotic formation of NMHCs, consequently resulting in a pronounced NMHCs emission in nearshore regions.

Assessing the effect of oceanic emission on NMHCs

Prior to delving into the correlation between oceanic emissions and NMHCs concentrations, it is imperative to acknowledge the influence of different gases' reactivity on this relationship. For instance, ethane possesses an atmospheric lifetime of approximately 78 d at 24 h [•OH] concentration of 6×10^5 molecules cm^{-3} (Jobson et al., 1999), using the rate constant with •OH at 288 K taken from Atkinson et al. (1997). The relatively long atmospheric residence time of ethane facilitates its accumulation in the atmosphere. Conversely, isoprene, with a much shorter lifetime of only 0.2 d, emitted within a very brief window can impact its atmospheric level. Thus, to mitigate the impact of varying reactivity among the different gas species, we calculated the lifetime-weighted concentrations of each NMHCs according to their atmospheric lifetime (introduced in section 2.5). This novel method is more nuanced to assess the impact of oceanic emission on atmospheric NMHCs, as it acknowledges not only their abundance but also their residence in the atmosphere.

18

419   Despite the elevated oceanic emission of NMHCs within the 100 km from land, its

420   impact on atmospheric NMHCs composition was comparatively weak displaying a

421   slope of 0.0187 (Fig. 5c), which was lower than the fitted result of the dataset in areas

422   beyond 100 km from land with a slope of 0.0415 (Fig. 5d). This could be attributed to

423   the disturbance of terrestrial outflow in nearshore areas, mitigating the direct impact of

424   oceanic emission on NMHCs. As it extended further from the land, the terrestrial

425   influence diminished. This, in turn, strengthens the regulatory impact of oceanic

426   emission on atmospheric NMHCs levels.

427   In addition, the average flux of total alkenes across the entire region was 163 ± 221

428   nmol m^{-2} d^{-1}, which was approximately 5 times higher than that of alkanes (32.2 ± 37.5

429   nmol m^{-2} d^{-1}). This substantial discrepancy indicates that alkanes and alkenes are

430   certainly influenced differently by oceanic emissions. The correlation between the

431   lifetime-weighted concentrations of alkenes and their fluxes was statistically significant

432   ($r = 0.548$, $n = 57$, $p < 0.001$), while it was insignificant for alkanes ($r = 0.113$, $n = 76$,

433    $p = 0.329$). When specific species of alkanes (Fig. 5e) and alkenes (Fig. 5f) were

434   separately plotted against their sea-to-air fluxes, alkenes exhibited a steeper slope of

435   0.0072 compared to the slope of 0.0044 for alkanes. This signifies that oceanic emission

436   has a more significant impact on atmospheric alkenes compared to alkanes, which

437   verifies our hypothesis as stated at the end of section 3.3.

438   3.5 Identification and apportionment of the sources of marine
439   atmospheric NMHCs

440   Source identification

441   Since the chemical compositions are largely controlled by the sources of emissions,

442   specific ratios of hydrocarbons have been widely employed to identify the sources of

443   NMHCs (Gilman et al., 2013; Rossabi and Helmig, 2018). For instance, elevated iso-

444   pentane/n-pentane ratios are indicative of the heavy influence of vehicular emissions

445   (2.2-3.8) and gasoline fuel evaporation (1.8-4.6) (Gentner et al., 2009; Jobson et al.,

446   2004; Liu et al., 2008; Russo et al., 2010). Conversely, the lower ratios indicate the

447   importance of tropical forest fires (0.43-0.57) (Andreae and Merlet, 2001; Rossabi and

448   Helmig, 2018), natural and oil gas operations (0.81-1.1) (Gilman et al., 2013; Swarthout

449   et al., 2013), and marine vessel exhaust (1.59-1.71) (Bourtsoukidis et al., 2019) in

450   controlling the chemical composition of NMHCs. In this study, a significant correlation

451   was observed between i-pentane and n-pentane (r = 0.67, $p < 0.01$) (Fig. 6), and the i-

452   pentane/n-pentane ratio spans a wider range from 0.89 to 2.46, suggesting that the

453   composition of NMHCs in the marginal seas of China is controlled by multiple sources

454   e.g., natural and oil gas operations, marine vessel exhaust, vehicular emissions, and

455   gasoline evaporation.

456   Furthermore, propane, i-butane, and n-butane exhibited strong intercorrelations (r =

457   0.52-0.95, $p < 0.05$). They also displayed strong correlations with ethane, i-pentane,

458   and n-pentane (r = 0.55-0.98, $p < 0.05$). These alkanes were recognized as the primary

459   components of liquid petroleum gases (Blake and Rowland, 1995), extensively utilized

460   as fuel in taxis, private cars, and public buses in China (Guo et al., 2017; Zhang et al.,

461   2015). Notably, C3-C5 alkanes also exhibited significant correlations with ethane (r =

462   0.55-0.72, $p < 0.05$) and carbon monoxide (r = 0.59-0.81, $p < 0.05$), while ethane and

463   carbon monoxide are acknowledged tracers for fossil fuel or biomass/biofuel

464   combustion and incomplete combustion, respectively (Lai et al., 2010; Tang et al., 2009;

465   Parrish et al., 2009). This indicated the contribution of vehicular emissions of liquid

466   petroleum gases and combustion of fossil fuel or biomass to light alkanes. Additionally,

467   strong correlations were observed among monocyclic aromatics (benzene, toluene,

468 ethylbenzene) (r = 0.67-0.83, $p < 0.05$). This finding was consistent with recent

469 emission inventory research identifying monocyclic aromatics as significant

470 constituents of ship exhaust (Xiao et al., 2018b; Wu et al., 2019). As for oceanic

471 emissions, we have presented the sea-to-air fluxes of NMHCs and discussed the

472 significant effect of oceanic emissions on NMHCs in Section 3.4. Multiple studies

473 highlighted that the ocean is one of the important sources of these gases (Kato et al.,

474 2007; Li et al., 2019; Mallik et al., 2013; Sahu et al., 2010; Rudolph and Johnen, 1990).

475 **Source apportionment**

476 The potential sources of the atmospheric NMHCs and their respective contributions

477 to each category were determined using the PMF model. Four isolate factors were

478 extracted according to their composition profiles depicted in Fig. 7a. These factors,

479 including industrial production, exhaust emission, terrestrial vegetation, and oceanic

480 ventilation, were identified based on chemical profiles in the literature.

481 Propane, i-butane, n-butane, i-pentane, n-pentane, and CFC-11 showed strong

482 loadings (> 70 %) on factor 1. The presence of propane, butanes, and pentanes suggests

483 the influence of the refinery activities (Buzcu and Fraser, 2006). Additionally, propane

484 has been recognized as a characteristic NMHCs derived from natural gas emissions and

485 butane is indicative of liquefied petroleum gas (LPG) (Guo et al., 2011; Tsai et al., 2006;

486 Hui et al., 2018; Ho et al., 2009). Moreover, CFC-11 is a typical artificial industrial

487 product. Subsequently, factor 1 was identified as a factor relating to industrial activities.

488 The profile of factor 2 showed strong loadings of benzene (72 %), toluene (57 %),

489 and ethylbenzene (64 %), along with moderate impacts of ethylene (34 %) and

490 propylene (32 %). Benzene emissions are notably associated with vehicle exhaust

491 (Zhang et al., 2013; Zhang et al., 2016) and considerable fractions of aromatics can be

492 emitted from ship exhaust during both berthing and cruising (Cooper, 2005; Xiao et al.,

493 2018a). C2-C4 alkenes could stem from ship emissions in the open ocean (Eyring et al.,

494 2005). Therefore, factor 2 can be potentially assigned as a source of the exhaust

495 emissions of vehicles and ships.

496 Factor 3 was assigned as oceanic ventilation due to elevated percentages of DMS

497 (74 %) and $CHBr_3$ (53 %), considering the dominant contributions of ocean emission

498 to DMS (Lana et al., 2011; Lee and Brimblecombe, 2016) and $CHBr_3$ (Quack and

499 Wallace, 2003; Ashfold et al., 2014). Factor 4 was mainly characterized by a high

500 percentage of isoprene (68 %), an indicator of biogenic emission from terrestrial

501 vegetation (Guenther et al., 2006; Wu et al., 2016). However, given isoprene's high

502 reactivity, this factor should be treated cautiously and regarded as a lower limit (Fujita,

503 2001). Although its short atmospheric lifetime hinders long-range transport, the

504 minimum air mass transport time from land to the oceanic station was four hours in this

505 study, implying the potential for terrestrial isoprene to reach the nearshore atmosphere.

506 According to the results of the PMF model analysis, the dominant source of

507 atmospheric alkanes in the Chinese marginal seas was industrial activities (0.253 ppb,

508 60.8 %), followed by exhaust emissions (0.095 ppb, 23 %). Contributions from

509 terrestrial vegetation emission (0.049 ppb, 11 %) and oceanic ventilation (0.021 ppb,

510 5.2 %) were relatively smaller. Furthermore, exhaust emissions (0.017 ppb, 32.5 %),

511 industrial activities (0.017 ppb, 31 %), and ocean ventilation (0.016 ppb, 30.4 %)

512 contribute almost equally to atmospheric alkenes. Collectively, these three factors

513 constitute the main sources of alkenes (93.8 %), whereas the contribution from

514 terrestrial vegetation is minimal, at merely 6.2 %. Particularly, the contribution of

515 terrestrial sources to alkanes (89 %) is greater than that to alkenes (69.6 %), while the

516 contribution of ocean emission to alkenes (30.4 %) is greater than that to alkanes

(5.2 %). This is consistent with the conclusions in section 3.3 and section 3.4.

It must be acknowledged that the classification and quantification results derived from the PMF model inevitably involve uncertainties that are challenging to ascertain precisely. These uncertainties are primarily attributed to factors such as the number of gas species, the number of samples, and the temporal and spatial resolutions of sampling. It is noteworthy, however, the PMF analysis results are relatively consistent with the phenomena described in Sections 3.3 and 3.4. This consistency to some extent validates the accuracy of the PMF analysis and underscores the significant contribution and impact of terrestrial inputs on the atmospheric NMHCs in the marginal seas of China.

Contributions of terrestrial/oceanic NMHCs to SOA and ozone

The P_{SOAP} of C2-C5 NMHCs in the atmosphere over the Chinese marginal seas was 0.41 ± 0.18 µg m^{-3}, with terrestrial sources contributing the majority (0.32 ± 0.14 µg m^{-3}), accounting for approximately 78% (Fig. 8a). Specifically, the P_{SOAP} from terrestrial alkanes and alkenes were 0.17 ± 0.07 and 0.15 ± 0.06 µg m^{-3}, respectively, while marine sources contributed 0.02 ± 0.01 and 0.07 ± 0.03 µg m^{-3} for alkanes and alkenes, respectively. Additionally, troposphere aerosol concentrations over the Chinese marginal seas during the investigation period were calculated using data from the NASA Goddard Earth Sciences Data and Information Services Center (GES DISC), ranging from 0.77 to 3.98 µg m^{-3}, with an average of 1.80 ± 0.71 µg m^{-3}. The aerosol concentrations decreased from the coastal areas towards the open sea (Fig. 8b), suggesting an obvious influence of terrestrial inputs on the aerosol levels in the coastal atmosphere. Based on the remote sensing data, it is roughly estimated that terrestrial C2-C5 NMHCs contribute ~18% to the total aerosol concentration, indicating their non-

negligible role in influencing the atmospheric aerosol levels over the marginal seas.

Similarly, the OFP of alkanes and alkenes from terrestrial sources were 2.35 ± 1.01 and 1.18 ± 0.51 µg m^{-3}, respectively, significantly higher than those from marine sources (0.14 ± 0.06 µg m^{-3} for alkanes and 0.50 ± 0.21 µg m^{-3} for alkenes) (Fig. 8c). However, the ozone distribution in the offshore atmosphere of China showed a decreasing trend from north to south (Fig. 8d). The marine atmosphere generally acts as a net ozone sink with ozone being primarily removed by photochemical degradation (Monks et al., 1998; Conley et al., 2011). The increasing solar radiation intensity from north to south enhances ozone degradation rates, likely dominating the ozone distribution in China's offshore atmosphere. Notably, satellite observations (GES DISC) during this investigation period indicated that the tropospheric ozone was approximately 82.6 ± 3.08 µg m^{-3} over the Chinese marginal seas. Among this, terrestrial C2-C5 NMHCs contributed around 4% to total ozone concentration, suggesting a certain impact of terrestrial outflow on the tropospheric ozone in these regions.

4 Conclusions

Our study characterized the atmospheric NMHCs in both coastal cities and Chinese marginal seas, and determined that both oceanic ventilation and terrestrial inputs play important roles in controlling the distribution and chemical composition of NMHCs in the coastal atmosphere of China.

Alkanes were the dominant NMHCs both in urban and nearshore atmospheres, and the atmospheric concentrations of alkanes were significantly higher in coastal cities compared to coastal seas, showing the potential of terrestrial alkanes as a source of alkanes in the marine atmosphere through transport. Generally, alkane concentrations

tended to be higher in cases: sampling sites closer to land, longer retention of air mass over land, and shorter air mass transport time from land to sampling site. However, these effects could not apply to alkenes due to their higher reactivities and the substantial sea-to-air fluxes. Additionally, the impact of oceanic emissions on NMHCs composition was more pronounced in areas beyond 100 km from land compared to areas within 100 km, because the terrestrial input gradually diminishes along the direction towards the open ocean.

Combining the outcomes of the PMF model and chemical profiles of diverse sources in the literature, we extracted four isolated sources of NMHCs in the nearshore atmosphere. Terrestrial sources (including industrial activities, vehicular exhaust, and vegetation emission) primarily constitute the NMHCs in the nearshore atmospheres, and they partially influence atmospheric SOA and ozone levels. This indicates the potential importance of terrestrial outflow in shaping the air quality and regulating climate dynamics in the marginal seas.

Code and data availability

Data presented in this paper are publicly available at Figshare via https://doi.org/10.6084/m9.figshare.24722286. The remote-sensing datasets of Chl-*a* and total absorption at 443 nm are available at https://oceancolor.gsfc.nasa.gov, aerosol and ozone at https://goldsmr5.gesdisc.eosdis.nasa.gov. Code to calculate the retention of air mass over land can be downloaded from https://doi.org/10.1029/2021JD034960 (Zhou et al., 2021).

Competing interests

The authors declare that they have no conflict of interest.

Author contributions

Honghai Zhang and Jian Wang designed the investigation and experiments. Jian Wang, Qianyao Ma, Feng Xu, Gaobin Xu, Shibo Yan, Jiawei Zhang, and Jianlong Li collected and determined the samples. Jian Wang analyzed the data and wrote the manuscript. Honghai Zhang, Lei Xue, Zhaohui Chen, and Guiling Zhang reviewed and revised the manuscript.

Acknowledgments

Financial support

References

Andreae, M. O. and Merlet, P.: Emission of trace gases and aerosols from biomass burning, Glob. Biogeochem. Cycle, 15, 955-966, https://doi.org/10.1029/2000GB001382, 2001.

Ashfold, M. J., Harris, N. R. P., Manning, A. J., Robinson, A. D., Warwick, N. J., and Pyle, J. A.: Estimates of tropical bromoform emissions using an inversion method, Atmos. Chem. Phys., 14, 979-994, https://doi.org/10.5194/acp-14-979-2014, 2014.

Atkinson, R., Baulch, D. L., Cox, R. A., Hampson, R. F., Kerr, J. A., Rossi, M. J., and Troe, J.: Evaluated kinetic, photochemical and heterogeneous data for atmospheric chemistry .5. Iupac subcommittee on gas kinetic data evaluation for atmospheric chemistry, J. Phys. Chem. Ref. Data, 26, 521-1011, https://doi.org/10.1063/1.556011, 1997.

Blake, D. R. and Rowland, F. S.: Urban leakage of liquefied petroleum gas and its impact on Mexico City air quality, Science, 269, 953-956, https://doi.org/10.1126/science.269.5226.953, 1995.

Bonsang, B., Polle, C., and Lambert, G.: Evidence for marine production of isoprene, Geophys. Res. Lett., 19, 1129-1132, https://doi.org/10.1029/92GL00083, 1992.

Bourtsoukidis, E., Ernle, L., Crowley, J. N., Lelieveld, J., Paris, J. D., Pozzer, A., Walter, D., and Williams, J.: Non-methane hydrocarbon (c2-c8) sources and sinks around the Arabian Peninsula, Atmos. Chem. Phys., 19, 7209-7232, https://doi.org/10.5194/acp-19-7209-2019, 2019.

Broadgate, W. J., Liss, P. S., and Penkett, S. A.: Seasonal emissions of isoprene and other reactive hydrocarbon gases from the ocean, Geophys. Res. Lett., 24, 2675-2678, https://doi.org/10.1029/97GL02736, 1997.

Buzcu, B. and Fraser, M. P.: Source identification and apportionment of volatile organic compounds in Houston, TX, Atmos. Environ., 40, 2385-2400, https://doi.org/10.1016/j.atmosenv.2005.12.020, 2006.

Carter, W. P. L.: Development of a condensed SAPRC-07 chemical mechanism, Atmos. Environ., 44, 5336-5345, https://doi.org/10.1016/j.atmosenv.2010.01.024, 2010.

Carter, W. P. L.: Development of ozone reactivity scales for volatile organic compounds, J. Air Waste Manag. Assoc., 44, 881-899, https://doi.org/10.1080/1073161X.1994.10467290, 1994.

Conley, S. A., Faloona, I. C., Lenschow, D. H., Campos, T., Heizer, C., Weinheimer, A., Cantrell, C. A., Mauldin, R. L., Hornbrook, R. S., Pollack, I., and Bandy, A: A complete dynamical ozone budget measured in the tropical marine boundary layer during PASE, J. Atmos. Chem., 66, 55-70, https://doi.org/10.1007/s10874-011-9195-0, 2011.

Cooper, D. A.: Hcb, pcb, pcdd and pcdf emissions from ships, Atmos. Environ., 39, 4901-4912, https://doi.org/10.1016/j.atmosenv.2005.04.037, 2005.

Decesari, S., Paglione, M., Rinaldi, M., Dall'Osto, M., Simó, R., Zanca, N., Volpi, F., Facchini, M. C., Hoffmann, T., Götz, S., Kampf, C. J., O'Dowd, C., Ceburnis, D., Ovadnevaite, J., and Tagliavini, E.: Shipborne measurements of antarctic submicron organic aerosols: An NMR perspective linking multiple sources and bioregions, Atmos. Chem. Phys., 20, 4193-4207, https://doi.org/10.5194/acp-20-4193-2020, 2020.

Ding, A., Wang, T., Zhao, M., Wang, T., and Li, Z. K.: Simulation of sea-land breezes and a discussion of their implications on the transport of air pollution during a multi-day ozone episode in the Pearl River Delta of China, Atmos. Environ., 38, 6737-6750, https://doi.org/10.1016/j.atmosenv.2004.09.017, 2004.

Eyring, V., Kohler, H. W., van Aardenne, J., and Lauer, A.: Emissions from international shipping: 1. The last 50 years, J. Geophys. Res.-Atmos., 110, https://doi.org/10.1029/2004JD005619, 2005.

Fujita, E. M.: Hydrocarbon source apportionment for the 1996 Paso del Norte Ozone Study, Sci. Total Environ., 276, 171-184, https://doi.org/10.1016/S0048-9697(01)00778-1, 2001.

Gentner, D. R., Harley, R. A., Miller, A. M., and Goldstein, A. H.: Diurnal and seasonal variability of gasoline-related volatile organic compound emissions in riverside, California, Environ. Sci. Technol., 43, 4247-4252, https://doi.org/10.1021/es9006228, 2009.

Gilman, J. B., Lerner, B. M., Kuster, W. C., and de Gouw, J. A.: Source signature of volatile organic compounds from oil and natural gas operations in Northeastern Colorado (vol 47, pg 1297, 2013), Environ. Sci. Technol., 47, 10094-10094, https://doi.org/10.1021/es4036978, 2013.

Grosjean, D. and Seinfeld, J.H.: Parameterization of the formation potential of secondary organic

aerosols. Atmos. Environ. 23, 1733–1747, https://doi.org/10.1016/0004-6981(89)90058-9, 1989.

Guenther, A., Karl, T., Harley, P., Wiedinmyer, C., Palmer, P. I., and Geron, C.: Estimates of global terrestrial isoprene emissions using MEGAN (model of emissions of gases and aerosols from nature), Atmos. Chem. Phys., 6, 3181-3210, https://doi.org/10.5194/acp-6-3181-2006, 2006.

Guenther, A., Hewitt, C. N., Erickson, D., Fall, R., Geron, C., Graedel, T., Harley, P., Klinger, L., Lerdau, M., McKay, W. A., Pierce, T., Scholes, B., Steinbrecher, R., Tallamraju, R., Taylor, J., and Zimmerman, P.: A global-model of natural volatile organic-compound emissions, J. Geophys. Res.-Atmos., 100, 8873-8892, https://doi.org/10.1029/94JD02950, 1995.

Guenther, A. B., Jiang, X., Heald, C. L., Sakulyanontvittaya, T., Duhl, T., Emmons, L. K., and Wang, X.: The Model of Emissions of Gases and Aerosols from Nature version 2.1 (MEGAN2.1): an extended and updated framework for modeling biogenic emissions, Geosci. Model Dev., 5, 1471–1492, https://doi.org/10.5194/gmd-5-1471-2012, 2012.

Guo, H., Cheng, H. R., Ling, Z. H., Louie, P. K. K., and Ayoko, G. A.: Which emission sources are responsible for the volatile organic compounds in the atmosphere of Pearl River Delta?, J. Hazard. Mater., 188, 116-124, https://doi.org/10.1016/j.jhazmat.2011.01.081, 2011.

Guo, H., Ling, Z. H., Cheng, H. R., Simpson, I. J., Lyu, X. P., Wang, X. M., Shao, M., Lu, H. X., Ayoko, G., Zhang, Y. L., Saunders, S. M., Lam, S. H. M., Wang, J. L., and Blake, D. R.: Tropospheric volatile organic compounds in China, Sci. Total Environ., 574, 1021-1043, https://doi.org/10.1016/j.scitotenv.2016.09.116, 2017.

Hallquist, M., Wenger, J. C., Baltensperger, U., Rudich, Y., Simpson, D., Claeys, M., Dommen, J., Donahue, N. M., George, C., Goldstein, A. H., Hamilton, J. F., Herrmann, H., Hoffmann, T., Iinuma, Y., Jang, M., Jenkin, M. E., Jimenez, J. L., Kiendler-Scharr, A., Maenhaut, W., McFiggans, G., Mentel, T. F., Monod, A., Prevot, A. S. H., Seinfeld, J. H., Surratt, J. D., Szmigielski, R., and Wildt, J.: The formation, properties and impact of secondary organic aerosol: Current and emerging issues, Atmos. Chem. Phys., 9, 5155-5236, https://doi.org/10.5194/acp-9-5155-2009, 2009.

He, Z. R., Wang, X. M., Ling, Z. H., Zhao, J., Guo, H., Shao, M., and Wang, Z.: Contributions of different anthropogenic volatile organic compound sources to ozone formation at a receptor

site in the Pearl River Delta region and its policy implications, Atmos. Chem. Phys., 19, 8801-8816, https://doi.org/10.5194/acp-19-8801-2019, 2019.

Ho, K. F., Lee, S. C., Ho, W. K., Blake, D. R., Cheng, Y., Li, Y. S., Ho, S. S. H., Fung, K., Louie, P. K. K., and Park, D.: Vehicular emission of volatile organic compounds (VOCs) from a tunnel study in Hong Kong, Atmos. Chem. Phys., 9, 7491-7504, https://doi.org/10.5194/acp-9-7491-2009, 2009.

Houweling, S., Dentener, F., and Lelieveld, J.: The impact of nonmethane hydrocarbon compounds on tropospheric photochemistry, J. Geophys. Res.-Atmos., 103, 10673-10696, https://doi.org/10.1029/97JD03582, 1998.

Hui, L., Liu, X., Tan, Q., Feng, M., An, J., Qu, Y., Zhang, Y., and Jiang, M.: Characteristics, source apportionment and contribution of vocs to ozone formation in Wuhan, Central China, Atmos. Environ., 192, 55-71, https://doi.org/10.1016/j.atmosenv.2018.08.042, 2018.

Jobson, B. T., McKeen, S. A., Parrish, D. D., Fehsenfeld, F. C., Blake, D. R., Goldstein, A. H., Schauffler, S. M., and Elkins, J. C.: Trace gas mixing ratio variability versus lifetime in the troposphere and stratosphere: Observations, J. Geophys. Res.-Atmos., 104, 16091-16113, https://doi.org/10.1029/1999JD900126, 1999.

Jobson, B. T., Parrish, D. D., Goldan, P., Kuster, W., Fehsenfeld, F. C., Blake, D. R., Blake, N. J., and Niki, H.: Spatial and temporal variability of nonmethane hydrocarbon mixing ratios and their relation to photochemical lifetime, J. Geophys. Res.-Atmos., 103, 13557-13567, https://doi.org/10.1029/97JD01715, 1998.

Jobson, B. T., Berkowitz, C. M., Kuster, W. C., Goldan, P. D., Williams, E. J., Fesenfeld, F. C., Apel, E. C., Karl, T., Lonneman, W. A., and Riemer, D.: Hydrocarbon source signatures in Houston, Texas: Influence of the petrochemical industry, J. Geophys. Res.-Atmos., 109, https://doi.org/10.1029/2004JD004887, 2004.

Kato, S., Pochanart, P., and Kajii, Y.: Measurements of ozone and nonmethane hydrocarbons at Chichi-jima island, a remote island in the Western Pacific: Long-range transport of polluted air from the Pacific rim region, Atmos. Environ., 35, 6021-6029, https://doi.org/10.1016/S1352-2310(01)00453-8, 2001.

Kato, S., Ui, T., Uematsu, M., and Kajii, Y.: Trace gas measurements over the Northwest Pacific

during the 2002 IOC cruise, Geochem. Geophys. Geosyst., 8, https://doi.org/10.1029/2006GC001241, 2007.

Kato, S., Kajii, Y., Itokazu, R., Hirokawa, J., Koda, S., and Kinjo, Y.: Transport of atmospheric carbon monoxide, ozone, and hydrocarbons from Chinese coast to Okinawa island in the Western Pacific during winter, Atmos. Environ., 38, 2975-2981, https://doi.org/10.1016/j.atmosenv.2004.02.049, 2004.

Lai, S. C., Baker, A. K., Schuck, T. J., van Velthoven, P., Oram, D. E., Zahn, A., Hermann, M., Weigelt, A., Slemr, F., Brenninkmeijer, C. A. M., and Ziereis, H.: Pollution events observed during caribic flights in the upper troposphere between South China and the Philippines, Atmos. Chem. Phys., 10, 1649-1660, https://doi.org/10.5194/acp-10-1649-2010, 2010.

Lana, A., Bell, T. G., Simo, R., Vallina, S. M., Ballabrera-Poy, J., Kettle, A. J., Dachs, J., Bopp, L., Saltzman, E. S., Stefels, J., Johnson, J. E., and Liss, P. S.: An updated climatology of surface dimethlysulfide concentrations and emission fluxes in the global ocean, Glob. Biogeochem. Cycle, 25, https://doi.org/10.1029/2010GB003850, 2011.

Lee, C. L. and Brimblecombe, P.: Anthropogenic contributions to global carbonyl sulfide, carbon disulfide and organosulfides fluxes, Earth-Sci. Rev., 160, 1-18, https://doi.org/10.1016/j.earscirev.2016.06.005, 2016.

Lee, R. F. and Baker, J.: Ethylene and ethane production in an estuarine river: Formation from the decomposition of polyunsaturated fatty acids, Mar. Chem., 38, 25-36, https://doi.org/10.1016/0304-4203(92)90065-I, 1992.

Li, J. L., Zhai, X., Ma, Z., Zhang, H. H., and Yang, G. P.: Spatial distributions and sea-to-air fluxes of non-methane hydrocarbons in the atmosphere and seawater of the Western Pacific Ocean, Sci. Total Environ., 672, 491-501, https://doi.org/10.1016/j.scitotenv.2019.04.019, 2019.

Li, J. L., Zhai, X., Wu, Y. C., Wang, J., Zhang, H. H., and Yang, G. P.: Emissions and potential controls of light alkenes from the marginal seas of China, Sci. Total Environ., 758, https://doi.org/10.1016/j.scitotenv.2020.143655, 2021.

Li, L. Y., Xie, S. D., Zeng, L. M., Wu, R. R., and Li, J.: Characteristics of volatile organic compounds and their role in ground-level ozone formation in the Beijing-Tianjin-Hebei region, China, Atmos. Environ., 113, 247-254, https://doi.org/10.1016/j.atmosenv.2015.05.021, 2015.

748   Liu, B. S., Liang, D. N., Yang, J. M., Dai, Q. L., Bi, X. H., Feng, Y. C., Yuan, J., Xiao, Z. M., Zhang,

749   Y. F., and Xu, H.: Characterization and source apportionment of volatile organic compounds

750   based on 1-year of observational data in Tianjin, China, Environ. Pollut., 218, 757-769,

751   https://doi.org/10.1016/j.envpol.2016.07.072, 2016.

752   Liu, Y., Shao, M., Fu, L., Lu, S., Zeng, L., and Tang, D.: Source profiles of volatile organic

753   compounds (VOCs) measured in China: Part i, Atmos. Environ., 42, 6247-6260,

754   https://doi.org/10.1016/j.atmosenv.2008.01.070, 2008.

755   Mallik, C., Lal, S., Venkataramani, S., Naja, M., and Ojha, N.: Variability in ozone and its precursors

756   over the bay of Bengal during post monsoon: Transport and emission effects, J. Geophys. Res.-

757   Atmos., 118, 10190-10209, https://doi.org/10.1002/jgrd.50764, 2013.

758   Messina, P., Lathière, J., Sindelarova, K., Vuichard, N., Granier, C., Ghattas, J., Cozic, A., and

759   Hauglustaine, D. A.: Global biogenic volatile organic compound emissions in the ORCHIDEE

760   and MEGAN models and sensitivity to key parameters, Atmos. Chem. Phys., 16, 14169–14202,

761   https://doi.org/10.5194/acp-16-14169-2016, 2016.

762   Monks, P. S., Carpenter, L. J., Penkett, S. A., Ayers, G. P., Gillett, R. W., Galbally, I. E., and Meyer,

763   C. P.: Fundamental ozone photochemistry in the remote marine boundary layer: the soapex

764   experiment, measurement and theory, Atmos. Environ., 32, 3647-3664,

765   https://doi.org/10.1016/S1352-2310(98)00084-3, 1998.

766   Paatero, P. and Tapper, U.: Positive matrix factorization - a nonnegative factor model with optimal

767   utilization of error-estimates of data values, Environmetrics, 5, 111-126,

768   https://doi.org/10.1002/env.3170050203, 1994.

769   Parrish, D. D., Kuster, W. C., Shao, M., Yokouchi, Y., Kondo, Y., Goldan, P. D., de Gouw, J. A.,

770   Koike, M., and Shirai, T.: Comparison of air pollutant emissions among mega-cities, Atmos.

771   Environ., 43, 6435-6441, https://doi.org/10.1016/j.atmosenv.2009.06.024, 2009.

772   Quack, B. and Wallace, D. W. R.: Air-sea flux of bromoform: Controls, rates, and implications, Glob.

773   Biogeochem. Cycle, 17, https://doi.org/10.1029/2002GB001890, 2003.

774   Ratte, M., Plassdulmer, C., Koppmann, R., and Rudolph, J.: Horizontal and vertical profiles of light-

775   hydrocarbons in sea-water related to biological, chemical and physical parameters, Tellus Ser.

776   B-Chem. Phys. Meteorol., 47, 607-623, https://doi.org/10.1034/j.1600-0889.47.issue5.8.x,

777   1995.

778   Ratte, M., Plassdulmer, C., Koppmann, R., Rudolph, J., and Denga, J.: Production mechanism of

779   c2-c4 hydrocarbons in seawater - field-measurements and experiments, Glob. Biogeochem.

780   Cycle, 7, 369-378, https://doi.org/10.1029/93gb00054, 1993.

781   Riemer, D. D., Milne, P. J., Zika, R. G., and Pos, W. H.: Photoproduction of nonmethane

782   hydrocarbons (NMHCs) in seawater, Mar. Chem., 71, 177-198, https://doi.org/10.1016/S0304-

783   4203(00)00048-7, 2000.

784   Rossabi, S. and Helmig, D.: Changes in atmospheric butanes and pentanes and their isomeric ratios

785   in the continental United States, J. Geophys. Res.-Atmos., 123, 3772-3790,

786   https://doi.org/10.1002/2017JD027709, 2018.

787   Rudolph, J. and Johnen, F. J.: Measurements of light atmospheric hydrocarbons over the Atlantic in

788   regions of low biological activity, J. Geophys. Res.-Atmos., 95, 20583-20591,

789   https://doi.org/10.1029/JD095iD12p20583, 1990.

790   Russo, R. S., Zhou, Y., White, M. L., Mao, H., Talbot, R., and Sive, B. C.: Multi-year (2004–2008)

791   record of nonmethane hydrocarbons and halocarbons in New England: Seasonal variations and

792   regional sources, Atmos. Chem. Phys., 10, 4909-4929, https://doi.org/10.5194/acp-10-4909-

793   2010, 2010.

794   Russo, R. S., Talbot, R. W., Dibb, J. E., Scheuer, E., Seid, G., Jordan, C. E., Fuelberg, H. E., Sachse,

795   G. W., Avery, M. A., Vay, S. A., Blake, D. R., Blake, N. J., Atlas, E., Fried, A., Sandholm, S.

796   T., Tan, D., Singh, H. B., Snow, J., and Heikes, B. G.: Chemical composition of Asian

797   continental outflow over the Western Pacific: Results from Transport and Chemical Evolution

798   over the Pacific (TRACE-P), J. Geophys. Res.-Atmos., 108,

799   https://doi.org/10.1029/2002JD003184, 2003.

800   Sahu, L. K., Lal, S., and Venkataramani, S.: Impact of monsoon circulations on oceanic emissions

801   of light alkenes over bay of Bengal, Glob. Biogeochem. Cycle, 24,

802   https://doi.org/10.1029/2009GB003766, 2010.

803   Sahu, L. K., Lal, S., and Venkataramani, S.: Seasonality in the latitudinal distributions of NMHCs

804   over bay of Bengal, Atmos. Environ., 45, 2356-2366,

805   https://doi.org/10.1016/j.atmosenv.2011.02.021, 2011.

Solomon, S., Thompson, D. W. J., Portmann, R. W., Oltmans, S. J., and Thompson, A. M.: On the distribution and variability of ozone in the tropical upper troposphere: Implications for tropical deep convection and chemical-dynamical coupling, Geophys. Res. Lett., 32, https://doi.org/10.1029/2005GL024323, 2005.

Sindelarova, K., Granier, C., Bouarar, I., Guenther, A., Tilmes, S., Stavrakou, T., Müller, J.-F., Kuhn, U., Stefani, P., and Knorr, W.: Global data set of biogenic VOC emissions calculated by the MEGAN model over the last 30 years, Atmos. Chem. Phys., 14, 9317–9341, https://doi.org/10.5194/acp-14-9317-2014, 2014.

Singh, H. B. and Zimmerman, P.: Atmospheric distributions and sources of non-methane hydrocarbons, Nriagu, J. O. (Ed.), Gaseous Pollutants: Characterisation and Cycling, Wiley, New York, p. 235, 1992.

Song, J. W., Zhang, Y. Y., Zhang, Y. L., Yuan, Q., Zhao, Y., Wang, X. M., Zou, S. C., Xu, W. H., and Lai, S. C.: A case study on the characterization of non-methane hydrocarbons over the South China Sea: Implication of land-sea air exchange, Sci. Total Environ., 717, https://doi.org/10.1016/j.scitotenv.2019.134754, 2020.

Song, Y., Shao, M., Liu, Y., Lu, S. H., Kuster, W., Goldan, P., and Xie, S. D.: Source apportionment of ambient volatile organic compounds in Beijing, Environ. Sci. Technol., 41, 4348-4353, https://doi.org/10.1021/es0625982, 2007.

Swarthout, R. F., Russo, R. S., Zhou, Y., Hart, A. H., and Sive, B. C.: Volatile organic compound distributions during the NACHTT campaign at the Boulder Atmospheric Observatory: Influence of urban and natural gas sources, J. Geophys. Res.-Atmos., 118, 10,614-610,637, https://doi.org/10.1002/jgrd.50722, 2013.

Talbot, R., Dibb, J., Scheuer, E., Seid, G., Russo, R., Sandholm, S., Tan, D., Singh, H., Blake, D., Blake, N., Atlas, E., Sachse, G., Jordan, C., and Avery, M.: Reactive nitrogen in Asian continental outflow over the western Pacific: Results from the NASA Transport and Chemical Evolution over the Pacific (TRACE-P) airborne mission, J. Geophys. Res.-Atmos., 108, https://doi.org/10.1029/2002JD003129, 2003.

Tang, J. H., Chan, L. Y., Chang, C. C., Liu, S., and Li, Y. S.: Characteristics and sources of non-methane hydrocarbons in background atmospheres of eastern, southwestern, and southern

China, J. Geophys. Res.-Atmos., 114, https://doi.org/10.1029/2008JD010333, 2009.

Tran, S., Bonsang, B., Gros, V., Peeken, I., Sarda-Esteve, R., Bernhardt, A., and Belviso, S.: A survey of carbon monoxide and non-methane hydrocarbons in the Arctic Ocean during summer 2010, Biogeosciences, 10, 1909-1935, https://doi.org/10.5194/bg-10-1909-2013, 2013.

Tsai, W. Y., Chan, L. Y., Blake, D. R., and Chu, K. W.: Vehicular fuel composition and atmospheric emissions in South China: Hong Kong, Macau, Guangzhou, and Zhuhai, Atmos. Chem. Phys., 6, 3281-3288, https://doi.org/10.5194/acp-6-3281-2006, 2006.

Wang, T., Ding, A. J., Blake, D. R., Zahorowski, W., Poon, C. N., and Li, Y. S.: Chemical characterization of the boundary layer outflow of air pollution to Hong Kong during february-april 2001, J. Geophys. Res.-Atmos., 108, https://doi.org/10.1029/2002JD003272, 2003.

Wang, T., Guo, H., Blake, D. R., Kwok, Y. H., Simpson, I. J., and Li, Y. S.: Measurements of trace gases in the inflow of South China Sea background air and outflow of regional pollution at Tai O, Southern China, J. Atmos. Chem., 52, 295-317, https://doi.org/10.1007/s10874-005-2219-x, 2005.

Wanninkhof, R.: Relationship between wind-speed and gas-exchange over the ocean, J. Geophys. Res.-Oceans, 97, 7373-7382, https://doi.org/10.1029/92jc00188, 1992.

Warneke, C. and de Gouw, J. A.: Organic trace gas composition of the marine boundary layer over the Northwest Indian Ocean in april 2000, Atmos. Environ., 35, 5923-5933, https://doi.org/10.1016/S1352-2310(01)00384-3, 2001.

Wilke, C. R. and Chang, P.: Correlation of diffusion coefficients in dilute solutions, AIChE Journal, 1, 264-270, https://doi.org/10.1002/aic.690010222, 1955.

Willis, M. D., Köllner, F., Burkart, J., Bozem, H., Thomas, J. L., Schneider, J., Aliabadi, A. A., Hoor, P. M., Schulz, H., Herber, A. B., Leaitch, W. R., and Abbatt, J. P. D.: Evidence for marine biogenic influence on summertime arctic aerosol, Geophys. Res. Lett., 44, 6460-6470, https://doi.org/10.1002/2017GL073359, 2017.

Wong, H. L. A., Wang, T., Ding, A., Blake, D. R., and Nam, J. C.: Impact of Asian continental outflow on the concentrations of O3, CO, NMHCs and halocarbons on Jeju Island, South Korea during march 2005, Atmos. Environ., 41, 2933-2944, https://doi.org/10.1016/j.atmosenv.2006.12.030, 2007.

Wu, D., Ding, X., Li, Q., Sun, J., Huang, C., Yao, L., Wang, X., Ye, X., Chen, Y., He, H., and Chen, J.: Pollutants emitted from typical Chinese vessels: Potential contributions to ozone and secondary organic aerosols, J. Clean. Prod., 238, 117862, https://doi.org/10.1016/j.jclepro.2019.117862, 2019.

Wu, F., Yu, Y., Sun, J., Zhang, J., Wang, J., Tang, G., and Wang, Y.: Characteristics, source apportionment and reactivity of ambient volatile organic compounds at Dinghu Mountain in Guangdong Province, China, Sci. Total Environ., 548-549, 347-359, https://doi.org/10.1016/j.scitotenv.2015.11.069, 2016.

Wu, R. R. and Xie, S. D.: Spatial distribution of secondary organic aerosol formation potential in China derived from speciated anthropogenic volatile organic compound emissions, Environ. Sci. Technol., 52, 8146-8156, https://doi.org/10.1021/acs.est.8b01269, 2018.

Wu, Y. C., Li, J. L., Wang, J., Zhuang, G. C., Liu, X. T., Zhang, H. H., and Yang, G. P.: Occurance, emission and environmental effects of non-methane hydrocarbons in the Yellow Sea and the East China Sea, Environ. Pollut., 270, 12, https://doi.org/10.1016/j.envpol.2020.116305, 2021.

Wu, Y. C., Gao, X. X., Zhang, H. H., Liu, Y. Z., Wang, J., Xu, F., Zhang, G. L., and Chen, Z. H.: Characteristics and emissions of isoprene and other non-methane hydrocarbons in the Northwest Pacific Ocean and responses to atmospheric aerosol deposition, Sci. Total Environ., 876, https://doi.org/10.1016/j.scitotenv.2023.162808, 2023.

Xiao, Q., Li, M., Liu, H., Fu, M., Deng, F., Lv, Z., Man, H., Jin, X., Liu, S., and He, K.: Characteristics of marine shipping emissions at berth: Profiles for particulate matter and volatile organic compounds, Atmos. Chem. Phys., 18, 9527-9545, https://doi.org/10.5194/acp-18-9527-2018, 2018a.

Xiao, Q., Li, M., Liu, H., Fu, M. L., Deng, F. Y., Lv, Z. F., Man, H. Y., Jin, X. X., Liu, S., and He, K. B.: Characteristics of marine shipping emissions at berth: Profiles for particulate matter and volatile organic compounds, Atmos. Chem. Phys., 18, 9527-9545, https://doi.org/10.5194/acp-18-9527-2018, 2018b.

Xu, G. B., Xu, F., Ji, X., Zhang, J., Yan, S. B., Mao, S. H., Yang, G. P.: Carbon monoxide cycling in the Eastern Indian Ocean. J. Geophys. Res.-Oceans, 128, e2022JC019411, https://doi.org/10.1029/2022JC019411.

36

Yuan, Q., Lai, S. C., Song, J. W., Ding, X., Zheng, L. S., Wang, X. M., Zhao, Y., Zheng, J. Y., Yue, D. L., Zhong, L. J., Niu, X. J., and Zhang, Y. Y.: Seasonal cycles of secondary organic aerosol tracers in rural Guangzhou, Southern China: The importance of atmospheric oxidants, Environ. Pollut., 240, 884-893, https://doi.org/10.1016/j.envpol.2018.05.009, 2018.

Zhang, Y., Zhi, Z., Li, X., Gao, J., and Song, Y.: Carboxylated mesoporous carbon microparticles as new approach to improve the oral bioavailability of poorly water-soluble carvedilol, Int. J. Pharm., 454, 403-411, https://doi.org/10.1016/j.ijpharm.2013.07.009, 2013.

Zhang, Y., Wang, X., Zhang, Z., Lü, S., Huang, Z., and Li, L.: Sources of c2–c4 alkenes, the most important ozone nonmethane hydrocarbon precursors in the Pearl River Delta region, Sci. Total Environ., 502, 236-245, https://doi.org/10.1016/j.scitotenv.2014.09.024, 2015.

Zhang, Z., Zhang, Y., Wang, X., Lü, S., Huang, Z., Huang, X., Yang, W., Wang, Y., and Zhang, Q.: Spatiotemporal patterns and source implications of aromatic hydrocarbons at six rural sites across China's developed coastal regions, J. Geophys. Res.-Atmos., 121, 6669-6687, https://doi.org/10.1002/2016JD025115, 2016.

Zhang, Z. J., Yan, X. Y., Gao, F. L., Thai, P., Wang, H., Chen, D., Zhou, L., Gong, D. C., Li, Q. Q., Morawska, L., and Wang, B. G.: Emission and health risk assessment of volatile organic compounds in various processes of a petroleum refinery in the Pearl River Delta, China, Environ. Pollut., 238, 452-461, https://doi.org/10.1016/j.envpol.2018.03.054, 2018.

Zhou, S. Q., Chen, Y., Paytan, A., Li, H. W., Wang, F. H., Zhu, Y. C., Yang, T. J., Zhang, Y., and Zhang, R. F.: Non-marine sources contribute to aerosol methanesulfonate over coastal seas, J. Geophys. Res.-Atmos., 126, https://doi.org/10.1029/2021JD034960, 2021.

Zou, Y. W., He, Z., Liu, C. Y., Qi, Q. Q., Yang, G. P., and Mao, S. H.: Coastal observation of halocarbons in the yellow sea and east china sea during winter: Spatial distribution and influence of different factors on the enzyme-mediated reactions, Environ. Pollut., 290, https://doi.org/10.1016/j.envpol.2021.118022, 2021.

922

923

924

925

926

Figure Captions


928
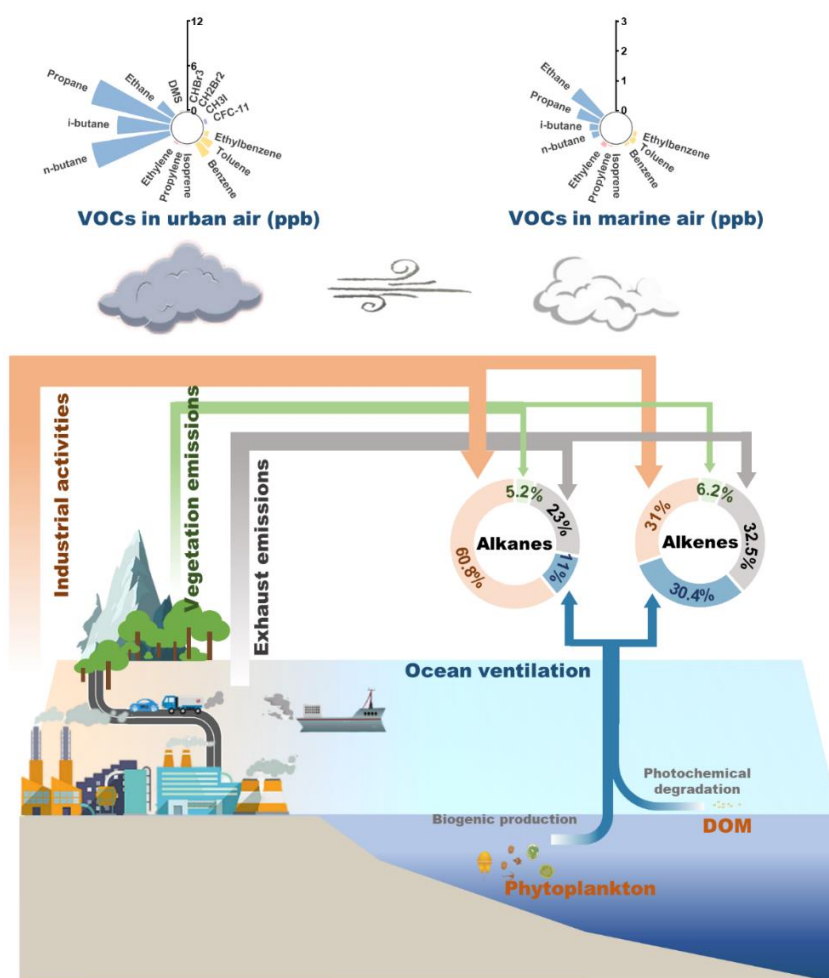
Graphical abstract Schematic diagram showing the main sources and their relative contributions to the NMHCs budget in the nearshore atmospheres of China. The ring bar chart above the land or the ocean shows the composition of urban or marine atmospheric trace gases determined in this study. The axes with units of ppb indicate the atmospheric concentrations of gases. The distinct colored wedges indicate the alkanes (skyblue), alkenes (pink), monocyclic aromatics (yellow),

VHCs (lilac), and DMS (palegreen). Note that only alkanes, alkenes, and monocyclic aromatics are shown in marine atmosphere. The colored arrows or annuli indicate the main sources of NMHCs in the offshore atmosphere: industrial activities (sandybrown), exhaust emissions (darkgray), oceanic ventilation (steelblue), and vegetation emissions (lightgreen). The numbers on the annuli are their respective relative contributions.
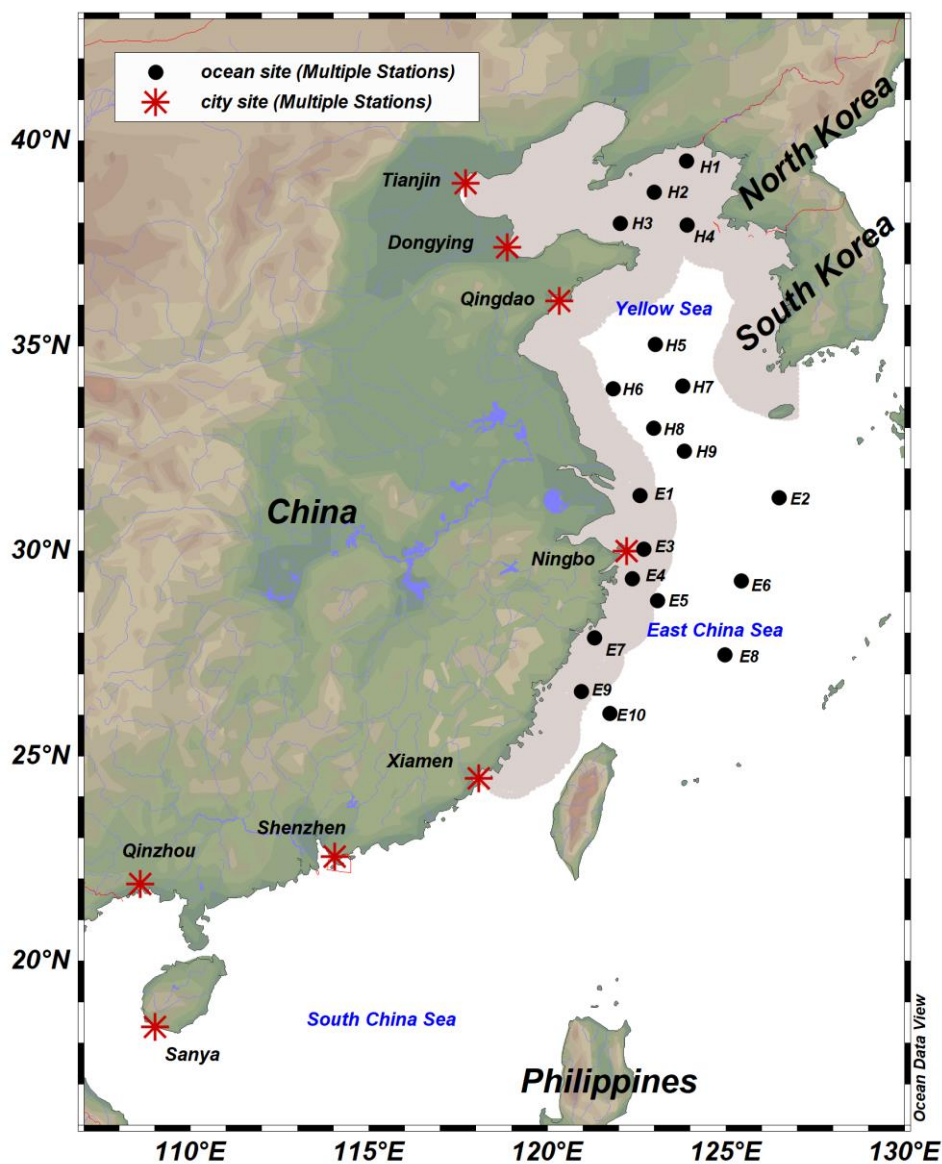
Figure 1 Map showing the sampling stations in the coastal cities (red asterisks) and marginal seas (black dots) of China from March to May 2021. The gray shaded area represents the inshore region within 100 km from the coastline.
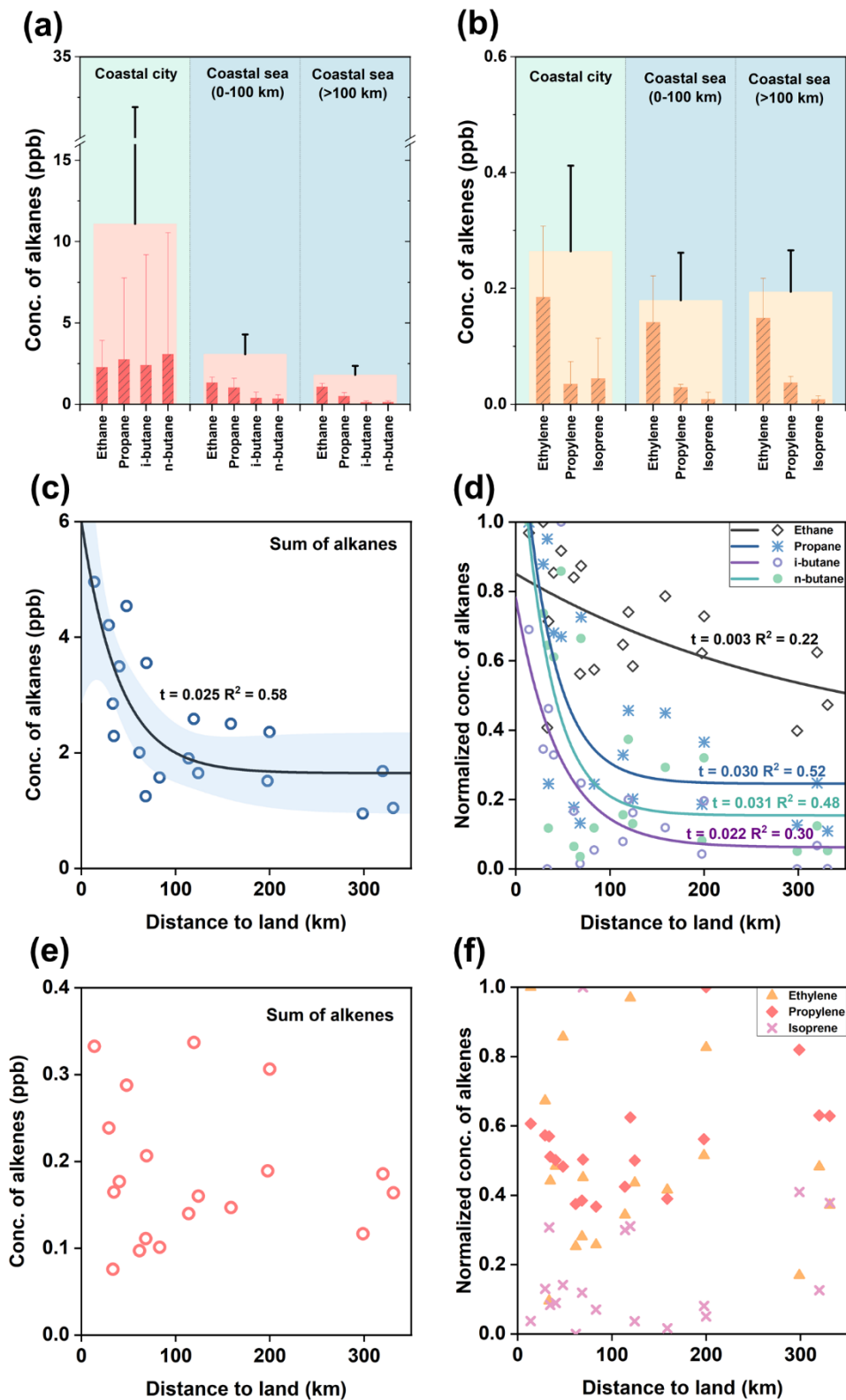
Figure 2 Means of the concentrations of alkanes (panel a) and alkenes (panel b) in the atmosphere

over coastal cities (n = 14) and nearshore (0-100 km, n = 10) and offshore (>100 km, n = 9) coastal

946   seas of China. The wider columns in panel a or b represent the sums of individual alkanes or alkenes

947   with error bars depicting the propagated errors from each NMHCs. Summed alkane (panel c) or

948   alkene (panel e) and normalized concentrations of specific alkane (panel d) or alkene (panel f)

949   plotted as a function ($y = Ae^{-tx}+y_0$) of the distance from sampling sites to the nearest land.

950

951
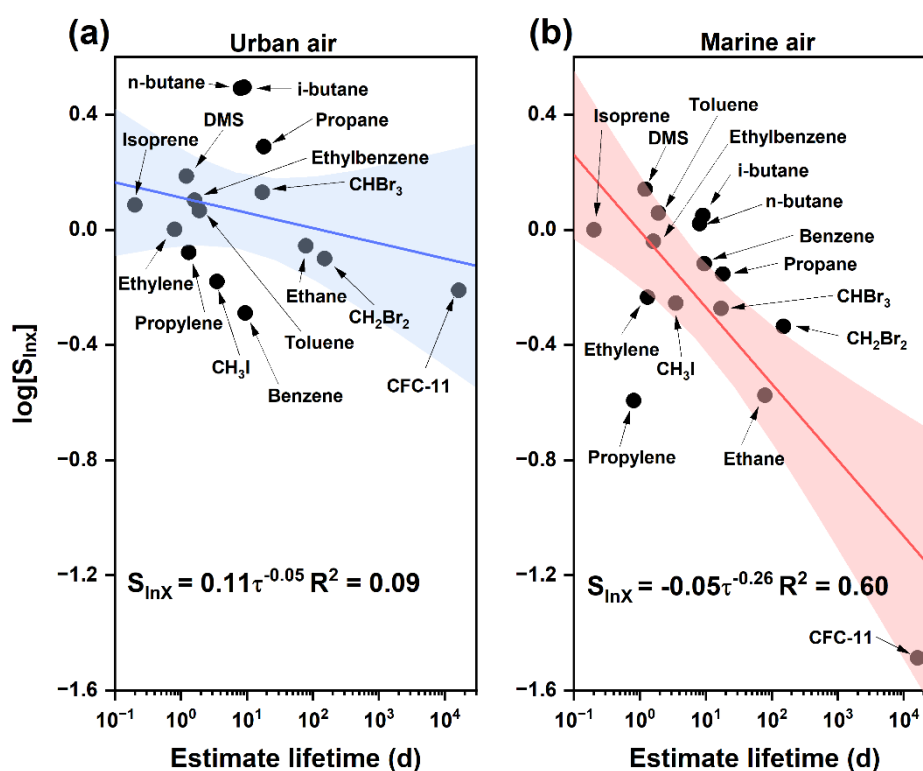
Figure 3 Atmospheric variability ($\log[S_{lnx}]$) plotted as a function of the estimated •OH lifetime for

953   each NMHCs from the coastal cities (panel a) and marginal seas of China (panel b). The blue or red

954   line is the best linear fitting. The shadowed area represents the confidence band at a 95 % confidence

955   level.

956
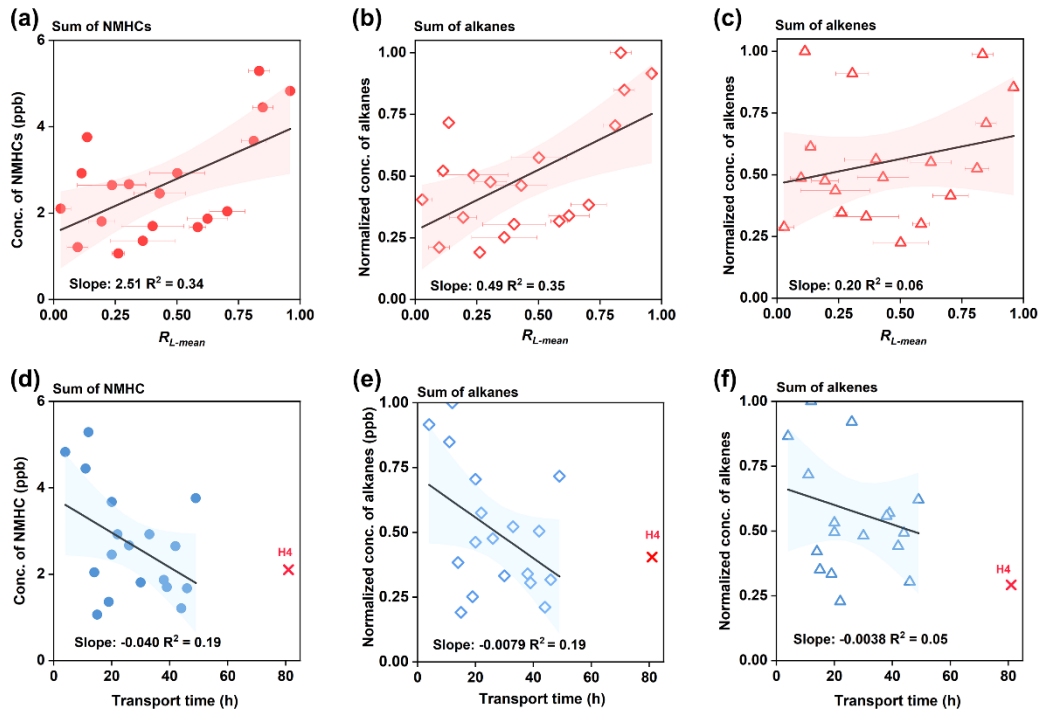
Figure 4 Concentrations of NMHCs combined (panel a or d), alkanes (panel b or e), and alkenes (panel c or f) at each site plotted against the mean retentions of air mass over land (R_{L-mean}, n = 3) or the transport time of air mass, respectively. The error bars for R_{L-mean} indicate the standard deviation from three different time-scale trajectories (48h, 72h, and 96h). The black line is the best fitting of the liner function and the shadowed area represents the confidence band at a 95 % confidence level. H4 (marked with red "×") is treated as an outlier since it alone deviates from the main dataset.
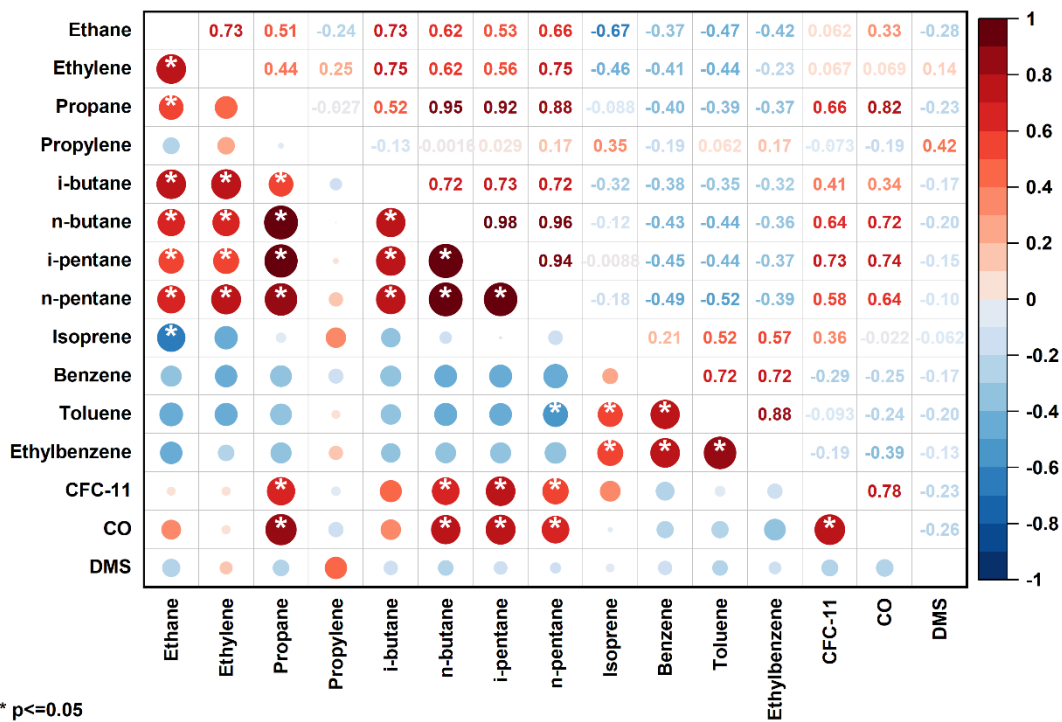
964
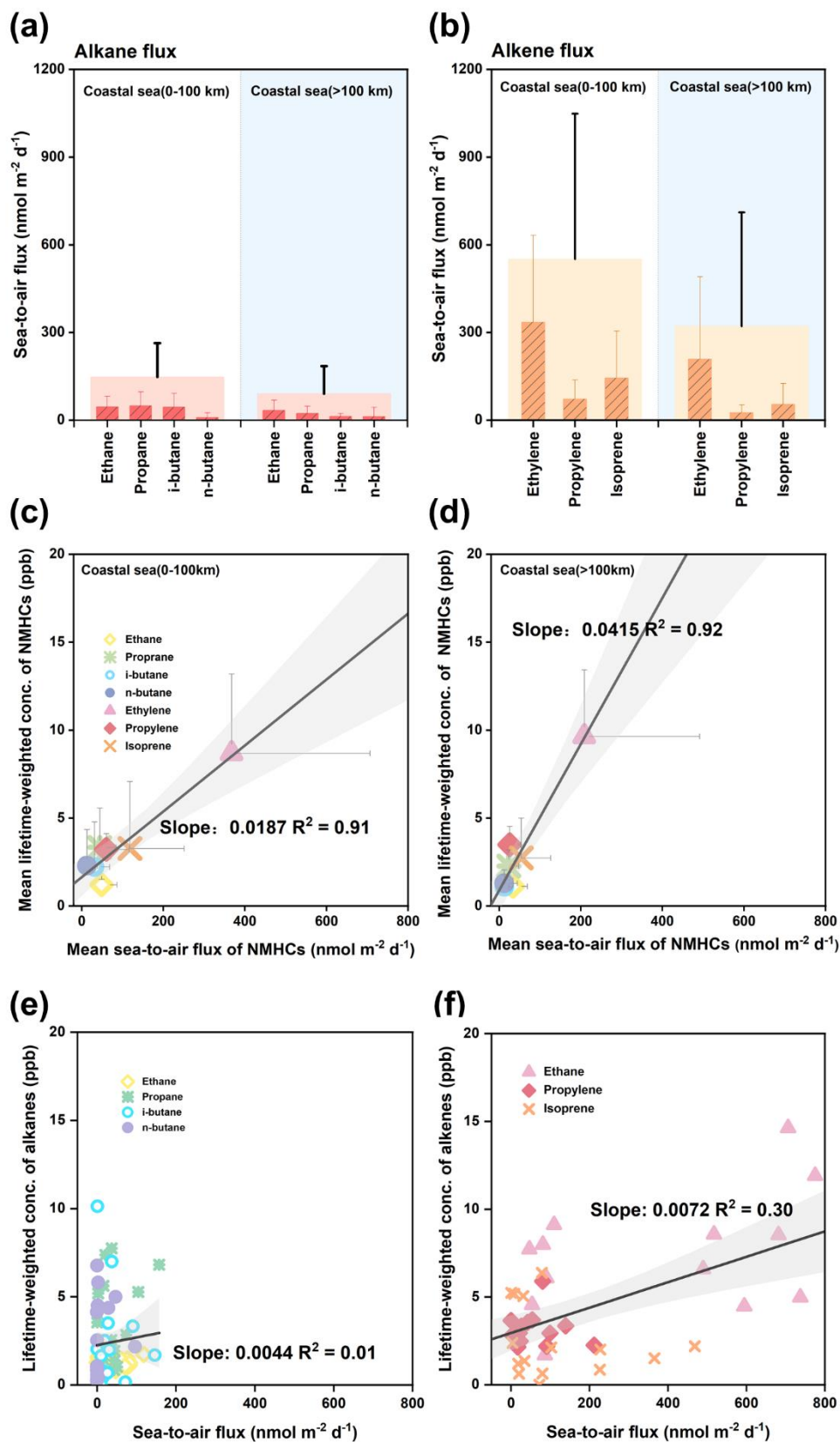
Figure 5 Means of sea-to-air fluxes of alkanes (panel a) and alkenes (panel b) in sea areas within

100 km (n = 10) and beyond 100 km (n = 9) from the nearshore land. The wider columns represent

the sum of alkanes or alkenes. Panel c or d shows the means of lifetime-weighted concentrations of

NMHCs plotted against the means of their mean sea-to-air fluxes in the area within 100 km or

beyond 100 km from the coastline. Specific lifetime-weighted concentrations of alkanes (panel e)

and alkenes (panel f) plotted against sea-to-air fluxes in the whole coastal sea region. The black,

blue or red line is the best linear fitting for each dataset and the shadowed area represents the

confidence band at a 95 % confidence level.

	Ethane	Ethylene	Propane	Propylene	i-butane	n-butane	i-pentane	n-pentane	Isoprene	Benzene	Toluene	Ethylbenzene	CFC-11	CO	DMS
Ethane		0.73	0.51	-0.24	0.73	0.62	0.53	0.66	-0.67	-0.37	-0.47	-0.42	0.062	0.33	-0.28
Ethylene			0.44	0.25	0.75	0.62	0.56	0.75	-0.46	-0.41	-0.44	-0.23	0.067	0.069	0.14
Propane				-0.027	0.52	0.95	0.92	0.88	-0.088	-0.40	-0.39	-0.37	0.66	0.82	-0.23
Propylene					-0.13	-0.0016	0.029	0.17	0.35	-0.19	0.062	0.17	-0.073	-0.19	0.42
i-butane						0.72	0.73	0.72	-0.32	-0.38	-0.35	-0.32	0.41	0.34	-0.17
n-butane							0.98	0.96	-0.12	-0.43	-0.44	-0.36	0.64	0.72	-0.20
i-pentane								0.94	-0.0008	-0.45	-0.44	-0.37	0.73	0.74	-0.15
n-pentane									-0.18	-0.49	-0.52	-0.39	0.58	0.64	-0.10
Isoprene										0.21	0.52	0.57	0.36	-0.022	-0.062
Benzene											0.72	0.72	-0.29	-0.25	-0.17
Toluene												0.88	-0.093	-0.24	-0.20
Ethylbenzene													-0.19	-0.39	-0.13
CFC-11														0.78	-0.23
CO															-0.26
DMS															

* p<=0.05

Figure 6 Correlation coefficients (*r*) between the various trace gases determined in the atmosphere

over the Yellow Sea and the East China Sea. The white asterisk means the correlation is significant

at the $p<0.05$ level. The color of dots, red or blue, indicates the positive or negative correlation and
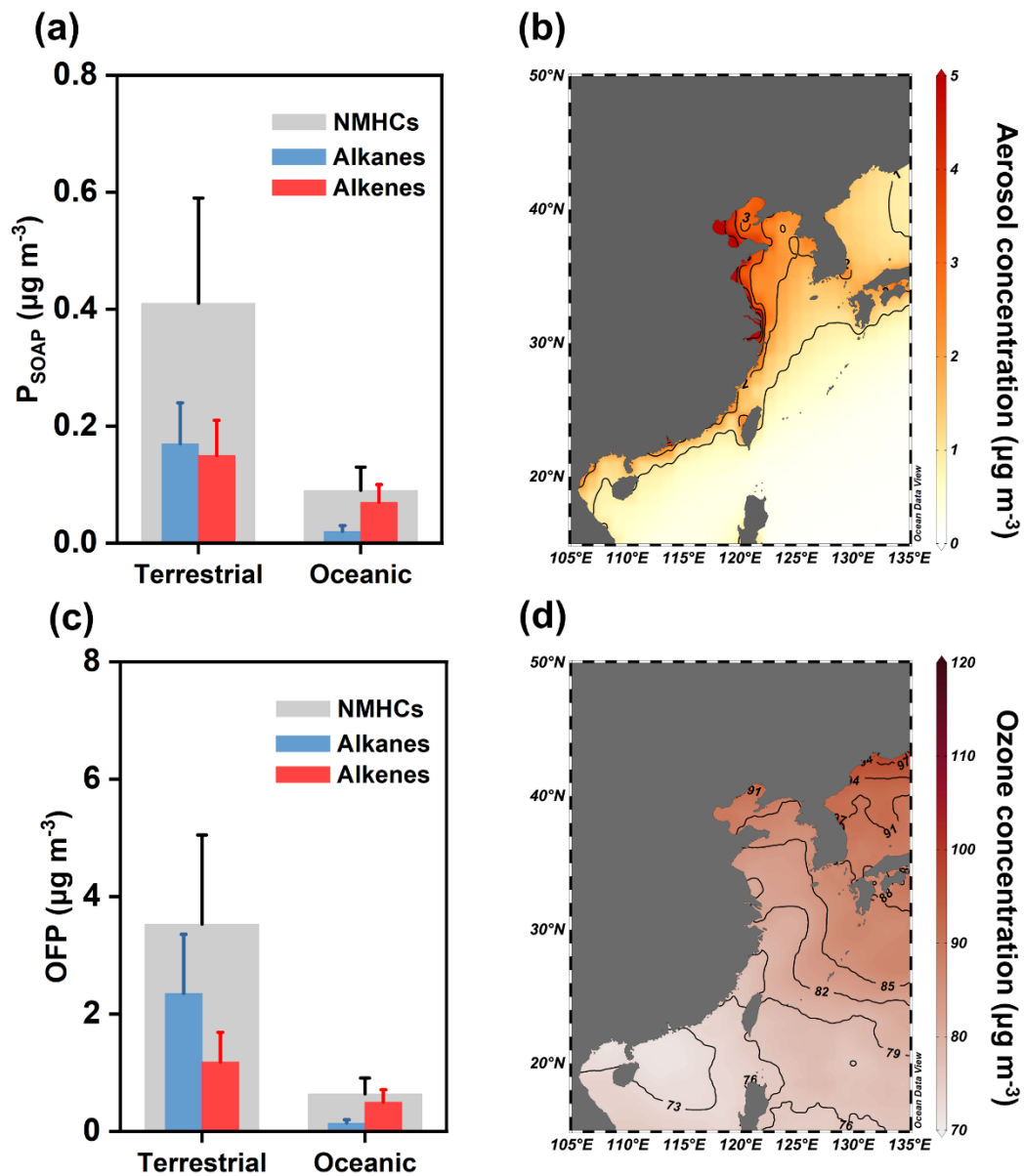
the size of the dots indicates the absolute value of *r*.
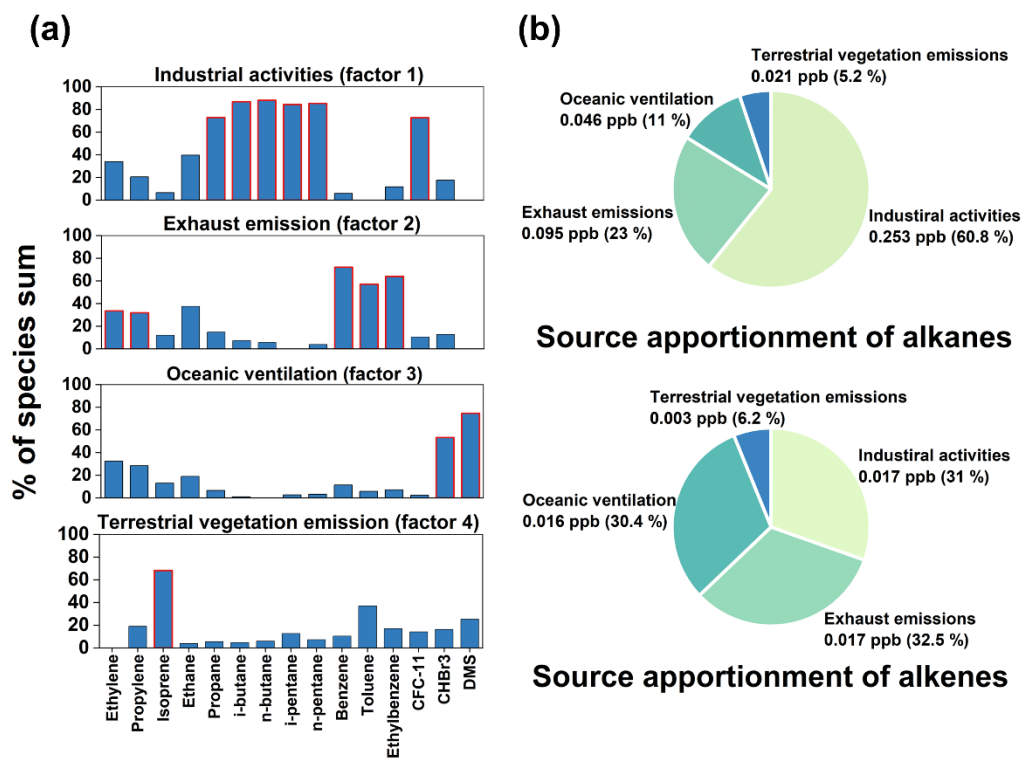
Figure 7 Representative factor profiles from the PMF model (panel a) and relative contributions of different factors/sources to the alkanes and alkenes in the oceanic atmosphere (panel b). NMHCs in panel a marked with red rim are selected as indicators for the specific factors.

983

Figure 8 OFP (panel a), P_{SOAP} (panel c) of NMHCs and averaged concentration of troposphere

aerosol (panel b), ozone (panel d) during the investigation period over the Chinese marginal seas.

Data of aerosol and ozone were downloaded from GES DISC

(https://goldsmr5.gesdisc.eosdis.nasa.gov/data/MERRA2/M2I3NPASM.5.12.4).

Table

Table 1 Atmospheric and seawater concentrations, sea-to-air fluxes, and the calculated atmospheric lifetime of each NMHCs based on the reaction with hydroxyl radicals (•OH).

Species	Conc. in urban air (ppb)	Conc. in oceanic air (ppb)	Conc. in seawater (pmol L^{-1})	Sea-to-air flux (nmol m^{-2} d^{-1})	Atmospheric lifetime [b] (d)
Ethane	2.26 (0.277-5.72)	1.24 (0.686-1.72)	11.6 (4.70-22.8)	44.6 (0.2-118)	78
Propane	2.95 (0.149-20.1)	0.822 (0.226-1.79)	12.6 (3.68-136)	41.5 (0.2-157)	18
i-butane	2.57 (BD[a]-27.6)	0.283 (BD-1.17)	9.46 (1.54-35.3)	31.7 (0.1-146)	9.1
n-butane	3.29 (0.018-30.2)	0.256 (0.025-0.694)	4.95 (BD-32.9)	10.9 (-0.8-96.1)	8.2
Ethylene	0.180 (0.035-0.390)	0.151 (0.028-0.295)	70.4 (8.40-136)	321 (1.7-775)	2.3
Propylene	0.036 (BD-0.129)	0.033 (0.022-0.060)	15.2 (2.42-27.6)	56.1 (0.2-212)	0.73
Isoprene	0.046 (0.006-0.250)	0.008 (BD-0.043)	31.0 (3.43-105)	112 (0.5-468)	0.19

[a]: Below the detection limit.

[b]: Assuming an average [•OH] of 6×10^5 molecules cm^{-3} within 24 h (Jobson et al., 1999), and using the rate constant with •OH at 288 K taken from Atkinson et al. (1997).